

Nuclear excitation functions for medical isotope production:  
Targeted radionuclide therapy via natIr(d,2n)<sup>193m</sup>Pt

Hannah Lovise Okstad Ekeberg

June 2020



# Contents

<b>1 Theory</b>	<b>5</b>
1.1 Treatment of cancer through radiative sources . . . . .	5
1.1.1 Targeted radionuclide therapy . . . . .	5
1.1.2 $^{193m}\text{Pt}$ as a potential therapeutic agent . . . . .	10
1.2 Radioactive decay law and Gamma-ray spectroscopy . . . . .	14
1.2.1 Radioactive decay law . . . . .	14
1.2.2 High purity Germanium detector . . . . .	15
1.2.3 Gamma-ray spectrum . . . . .	16
1.3 General nuclear reaction theory . . . . .	17
1.3.1 Nuclear reactions and reaction cross sections . . . . .	18
1.3.2 Energetic factors in nuclear reactions . . . . .	19
1.3.3 Nuclear cross sections . . . . .	23
1.3.4 Expected products from deuterions on iridium, iron, copper and nc . . . . .	24
1.4 From book . . . . .	24
1.5 The decay of the compound nucleus . . . . .	24
<b>2 Experimental setup</b>	<b>27</b>
2.1 Lawrence Berkeley National Laboratory's 88" Cyclotron . . . . .	27
2.2 The experiment . . . . .	27
2.2.1 Target design and foil characterization . . . . .	29
2.2.2 Irradiation of target stack . . . . .	29
2.2.3 Counting on high purity detectors . . . . .	32
<b>3 Analysis</b>	<b>35</b>
3.1 Gamma-ray spectroscopy . . . . .	35
3.2 Efficiency calibration . . . . .	37
3.3 End of beam activities . . . . .	38
3.4 Energy and Beam current . . . . .	39
3.4.1 Variance minimization . . . . .	41
<b>A Statistics</b>	<b>45</b>
<b>A Tables</b>	<b>47</b>
A.1 Product nuclei . . . . .	47

## CONTENTS

---

# Chapter 1

## Theory

### 1.1 Treatment of cancer through radiative sources

Today, multiple options are available for treatment of cancerous tissue, where some of the most commonly used methods are chemotherapy, surgery, immunotherapy, external beam-therapy, brachytherapy and targeted radionuclide therapy citation. The latter three treatment types utilize ionizing particles to induce damage in the DNA of cancerous cells, so that they undergo apoptosis. In external beam therapy, photons, electrons or hadrons are accelerated and sent towards a tumor externally, and in brachytherapy a contained radioactive source (with for instance a  $\beta^-$ -emitter), is placed in proximity to tumor. Targeted radionuclide therapy is an emerging alternative to the traditional treatment options, and offers a patient-specific treatment dependent on choice of radiopharmaceutical which targets a type of tumor or cell correct? need citation. A radiopharmaceutical consists of a radionuclide and a cell-targeting molecule called a tracer. Targeted radionuclide therapy utilizes the biochemical pathways in the body, thus with an appropriate tracer, targeted tissue with a high uptake of the radiopharmaceutical will receive a high dose, and healthy tissue can be spared (Yeong2014).

#### 1.1.1 Targeted radionuclide therapy

Write more detailed about what it is..

In treatment of diseases related to the use of radionuclides, there are multiple properties that play an important role, such as physical features like half-life, decay-mode, decay-products, radiation energy and linear energy transfer, and biochemical features like in tissue range, tissue targeting of tracer, uptake and retention in desired tissue, biological half-life and toxicity of radionuclide and decay-product (Yeong, therapeutic radionuclides in nuclear medicine). In addition, the availability, cost and quality is important, and that the production routes gives high isotopic purity of the product, along with high yield (Qaim, Nuclear Data for production of medical application of radionuclides: present status and future needs).

Here write about the various small things. Isotopic purity, half-life,

#### Particle interaction in matter

equation

$$Q_{\max} = \frac{4mME}{m + M}$$

can be from billiard physics, or inelastic collision physics. Also, bethe-block is proportional to

$$-\frac{dE}{dx} = 2\pi N_a r_e^2 m_e c^2 \rho \frac{Z}{A} \frac{z^2}{\beta^2} \left[ \ln \left( \frac{2m_e \gamma^2 v^2 Q_{\max}}{I^2} \right) - 2\beta^2 - \delta - 2\frac{C}{Z} \right] \quad (1.1)$$

where  $r_e$  is electron radius,  $m_e$  electron mass,  $N_a$  avogadro,  $I$  mean excitation potential,  $Z$  &  $A$  atomic number and mass number of absorbing material,  $\rho$  density of absorbing material,  $z$  charge of incident

particle,  $\beta = v/c$ ,  $\gamma = 1/\sqrt{1-\beta^2} = 1/\sqrt{1-v^2/c^2}$ ,  $\delta$  density correction, C shell correction,  $W_{\max}$  is max energy transfer per collision. In general,

$$\frac{dE}{dx} \propto \rho, \frac{z^2}{\beta^2}, \frac{Z}{A}$$

and logarithmic stuff which i dont know... so alpha particles are stopped quicker than protons if they have the same energy (Techniques for Nuclear and Particle physics experiments, p. 24). Particles interact differently in a given medium. Figure 1.1 shows how various particles interacts in a medium where the depth is on the x-axis and dose is on the y-axis. In a medium, there are positively charged nuclei and negatively charged electrons. We differ between neutral particles like neutrons and photons, and charged particles like electrons or protons, alpha-particles, and other heavy charged particles. Charged particles have a short range in comparison to neutral particles, as the Coulomb force forces the particle to interact continuously along the path, either either by scattering inelastically with the atomic electrons, or scattering elastically via the nuclei. Inelastic collisions is the dominant process, where the atomic electrons are either excited or ionized. If the now free electron had sufficient energy transferred from the incoming particle (called a  $\delta$ -electron), this electron can further ionize along the particle track. Elastic scattering is the less dominant process, where the energy loss is small, as long as the nuclei in the medium are larger than the incoming particle (Techniques for Nuclear and Particle Physics Experiments, William R. Leo, p. 21). The energy loss of heavy charged particles are described by an equation called Bethe-Block, where the energy loss at high energies is small since very little energy is transferred per collision with atomic electrons (due to the large mass). However, when the particle reaches low velocity, the particle interacts at a much higher rate in a very specific peak called the Bragg peak. Can be seen on figure 1.1, for the proton. As we can see, the energy deposited behind the tumor is zero, along with the energy deposition in front of the tumor is low which is something which can utilized in radiation therapy. However, since the Bragg peak is so narrow, a broadening of the beam might be necessary, which is to send out a beam of multiple energies, so that it is spread out. The dose in front of the tissue gets larger, but the dose behind is still zero. The electrons/positrons interacts differently, since the mass is equal to the atomic electrons, the energy transfer can be up to half of its mass, and it scatters like crazy. Electrons can experience energy loss either from collisions like heavy charged particles, or via the electromagnetic radiation that arises when electrons are losing energy (bremsstrahlung). However, for energies up to a few MeV, the collision energy loss dominates (Techniques for Nuclear and Particle Physics Experiments, William R. Leo, p. 37). On figure 1.1, we see that the electrons and proton interacts differently, there is no clear peak, and the incoming electrons immediately interacts with the medium, lose energy fast and the secondary electrons interacts after and slowly decreasing. At 22 MeV, bremsstrahlung stopping power is also evident, so we see an exponential tail which ....?

Photons interacts differently than charged particles. As they are neutral, they do not interact via inelastic collisions, but interacts via three different processes called photoelectric effect, compton scattering and pair production. Thus the energy is not degraded, and the beam can only be attenuated as a function of thickness  $x$  (Techniques for Nuclear and Particle Physics Experiments, William R. Leo, p. 53)

$$I(x) = I_0 e^{-\mu x} \quad (1.2)$$

where  $\mu$  is the attenuation coefficient. Photons can be gamma-rays or X-rays, where gamma-rays are produced in de-excitation of nuclei, and have ranges 0.1-10 MeV (Krane, p. 327), and X-rays can be either be produced in de-excitation of atomic electrons (where the energies are typically quite low), or be produced by de-accelerating fast electrons in an x-ray tube, for instance by hitting a material like tungsten, where the energy is high. As we can see on figure 1.1, the X-rays are produced in an x-ray tube (MV and kV is the voltage of the X-ray tube), and we can see that the 22 MV X-rays have a build-up effect, where ionized atomic electrons participates in increasing the dose, while the much lower 200 kV X-rays does only decrease. The gamma-rays from  $^{60}\text{Co}$  behaves similarly to the 200 kV X-rays, but are slightly higher in energy deposition as the energy in general are slightly higher

than 200 keV. The tale is exponential as we can see in eq. 1.2, and is in fact a problem in radiation therapy as the dose to healthy tissue behind the tumor is quite high.

Photoelectric effect dominates at lower energies, and happens when a photon (energy) is completely absorbed an atomic electron. In gamma-ray spectroscopy, this process is desired as the gamma-rays from nuclei is specific, and we can identify the nuclei on a spectrum. Probability of photoelectric effect is

$$\tau \propto \frac{Z^n}{E_\gamma^{3.5}}, \quad n = 4 \text{ or } 5 \quad (1.3)$$

where Z is the atomic number of material ((Techniques for Nuclear and Particle Physics Experiments, William R. Leo, p. 55).

In compton scattering, the photon has higher energy and can transfer parts of the energy to an atomic electron, be deflected and ionize further. The deflecting angle is dependent on energy, and the angle  $\theta \in (0^\circ, 180^\circ)$  (Techniques for Nuclear and Particle Physics Experiments, William R. Leo, p. 55-56). Compton scattering thus gives photons in a spectrum of different energies. This process is not desired in gamma-ray spectroscopy, and contributes to noise in a Compton region. This process is however desired in external radiation therapy, as the process gives rise to high energetic secondary electrons, and photons in which ionize further. The probability of interaction is

$$\sigma \propto Z \quad (1.4)$$

Pair production demands a photon energy to be equal or higher than two electron rest masses, as the photon is converted to an electron/positron pair ( $1.022 \text{ MeV} = 2m_0c^2$ ) (Techniques for Nuclear and Particle Physics Experiments, William R. Leo, p. 57). Probability of interaction is

$$\kappa \propto Z^2 \quad (1.5)$$

Finally neutrons interacts with the strong force with nuclei, and can be via absorption, or elastic or inelastic scattering. The interaction probability is dependent on energy, will not describe more. (Techniques for Nuclear and Particle Physics Experiments, William R. Leo, p. 64).

Whenever a charged particle like an electron or hadron enters a medium, the Coloumbforce will affect the charged particle and cause interactions with the atomic elecrtons. Neutral particles like photons and neutrons are not affected by the Coulomb force, thus interacts rarely. On figure ..., the 22 MV X-rays first has a build-up effect, where the initial photons induce ionizations and secondary electrons, which contributes to further ionization, and increases the dose. After, the dose decreases exponentially. The build-up effect for high-energetic photons which are only used in external beam therapy enables an energydependent maximum dose in tissue as a function of depth. However, the exponential tale gives dose to the healthy tissue behind. The gamma-rays in nuclei are not that energetic, and the lack of specificity does not make gamma-rays a suitable decay chain for therapeutic agents. Neutral particles interacts via absorption or

X-rays from an accelerator is produced by acceleration of electrons which hits a material like for instance wolfram or tungsten. The X-rays have energies ranging from zero to the max electron energy, and hence the X-ray energy is in MV instead of MeV. Why we are not using gamma-rays in treatment; range is too long, ionization are not frequent enough, and energy is too low?

#### The biological effect of ionizing radiation and linear energy transfer

**in general in this paragraph refer to the radiation biology book..** Ionizing radiation are particles with sufficient energy to cause ionizations along the particle track, thus separating an atom and one or more electrons **citation, maybe the bio-book?**. The free electron(s) can ionize further, and the positive ion can cause undesired reactions **find a citation**. DNA is a large molecule with two strands bound in a double helix structure. Each strand is composed of sugar and phosphate groups, and nitrogenous bases which bind the two strands. These bases are called adenin & guanin and cytosine & thyamin (always bound pairwise), and are bound through weak hydrogen bonds which are exposed to strand breaks. The cell is equipped with an impressive repair mechanism, and unless both DNA strands are

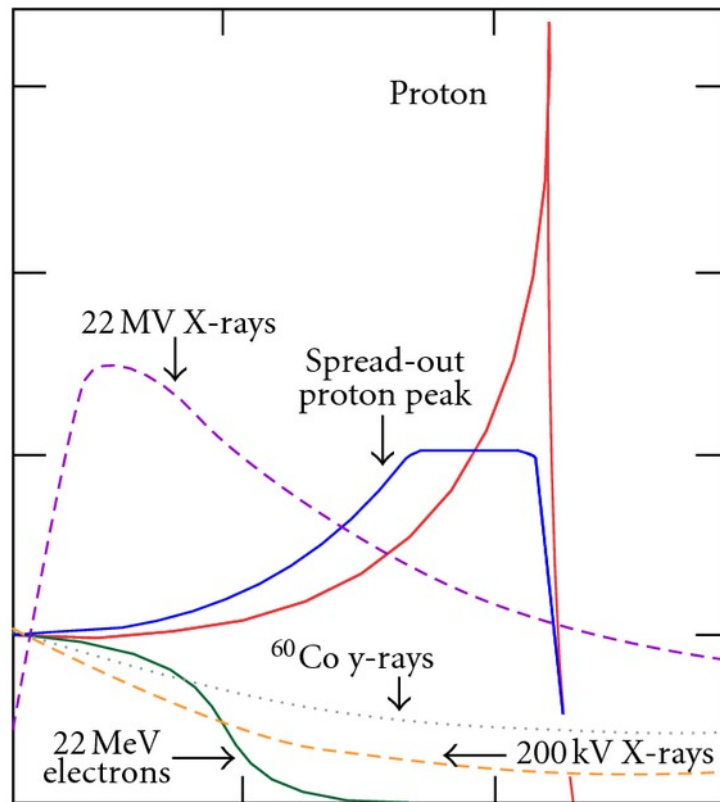


Figure 1.1: Medium depth along x-axis, energy deposition in tissue (or dose?) on y-axis. Find citation in special curriculum.

damaged, which is called a double stranded break (DSB), most damages are repaired [cite](#). Radiation damages in the DNA can be caused directly by the ionizing particle, or indirectly via free radicals which are subject to other ionizations. Since the body contains large amounts of water, ionization of water molecules giving for instance  $H^\bullet$  or  $OH^\bullet$  are important damaging factors. Damages induced in the DNA can be lethal to the cell and either cause apoptosis or mutation in which can be a cause of cancer. In therapy, the goal is to make the cancerous cells to undergo apoptosis, and choosing a particle which has a high probability of inducing damage will induce multiple double stranded breaks, if passing nearby.

Linear energy transfer (LET) describes the energy absorbed by the medium, and is defined as the average energy (typically measured in keV) deposited per unit length (typically measured in  $\mu\text{m}$ ) of the density material (book, p. 101):

$$\text{LET} = \frac{dE}{dx} \quad (1.6)$$

LET thus describes the general frequency in which a particle will deposit energy along the particle track. A particle with a high LET-value will interact more frequently over a shorter distance than a low LET-particle. In targeted radionuclide therapy, it is important that the range of the particle is short-range so that the healthy tissue is spared, and that the dose to the cancerous tumor is large. For therapy, medical isotopes which emit radiation with high LET such as  $\alpha$ ,  $\beta$  and auger-electrons are desired since the ionization rate is high and the distance traversed is low (Yeong, therapeutic radionuclides in nuclear medicine). Gamma-radiation is not a desired process in therapy as photons does not degrade in energy, thus can have a long range unless attenuated. Figure ... shows how alpha, beta and auger electrons interacts on the scale of DNA.

### Decay modes

Different decay modes have different ranges in the tissue. Dependent on the size of tumor, and critical tissue surrounding it, different emitters are used. However to reduce dose to healthy tissue, specific short range high LET particles are in general desired. Figure 1.2 shows the ranges of auger electrons, alpha-particles and  $\beta^-$ - particles on a cellular scale. The binding energy holds the nucleus together, and for unstable nuclei, the binding energy is so low that particles can be emitted to gain stability, lowering the binding energy. Beta and alpha decay changes the element, and the decay product is commonly in an excited state. Therefor gamma-decay commonly occurs after, and in gamma-ray spectroscopy, it is the gamma-rays of the de-excitation of the daughter which is detected. Knowledge about the energy and intensity of the radiation is very important. It is unrare that just one single process happens during a decay, and dependent on what the desired process is, there is a beta or alpha particle or gamma-rays, X-rays or auger electrons caused from electron capture or internal conversion. The ranges can be different.

Beta-decay happens whenever there is an overweight in number of protons or neutrons. For an overweight of neutrons,  $\beta^-$ -decay occurs, by transforming a neutron into a proton, a  $\beta^-$ -particle and an antineutrino



For an overweight in protons,  $\beta^+$  decay occurs, by transforming a proton into a neutron, a  $\beta^+$ -particle and a neutrino



$\beta^+$ -particles are typically used in diagnostic imaging in PET (positron emission tomography). Since neutron mass is higher than the proton mass (mass difference  $1.022 \text{ MeV}/c^2$ ), there is an additional threshold energy needed to induce the reaction. If the energy is not high enough, electron capture dominates, which takes in an atomic electron (typically from K-shell), and with a proton in the nucleus, transforming to a neutron and a neutrino:



Since beta-rays are not monoenergetic, the energy is distributed between three particles and gives a spectrum of different possible energies.  $\beta^-$ -emitters used in therapy are stopped rather quickly in tissue due to negative charge and low mass (as mentioned in the above section, energy transfer can be up to half of its mass. ),

Alpha-particles are  ${}^4\text{He}$ -nuclei, consisting of two protons and two neutrons. It is emitted from heavy nuclei. Since the nuclear force is short range (1fm ?), and heavy nuclei tend to be in the limit between electromagnetic and nuclear force, an alpha particles (which carries large binding energy) lowers the binding energy sufficiently so that the nucleus is more stable. The binding energy of an alpha particle is very high (28.3 MeV) which is why an alpha-particle is emitted to lower binding energy.

Gamma-decay is emission of photons following de-excitation of the nucleus, as de-excitation from one state to another. It is specific for the nucleus, and is thus called the fingerprint of the nucleus, because we can observe it for instance in a gamma-ray spectrum. Gamma-decay commonly occurs after beta or alpha decay, or can happen if there is an isomer, then the decay mode is called isomer transition. However, gamma-rays are not well suited in therapy themselves (however for imaging in SPECT more relevant). But nuclei that emit electrons following gamma-decay are more relevant. Internal conversion is a process where the gamma-ray interacts electromagnetically with atomic electrons, and the electron is emitted instead of the photon. This electron is called an conversion electron and has energy in the order of the gamma ray (minus atomic binding energy). In order to fill the atomic shells, a cascade of X-rays and auger electrons are emitted (auger electrons have energies in order of X-rays).

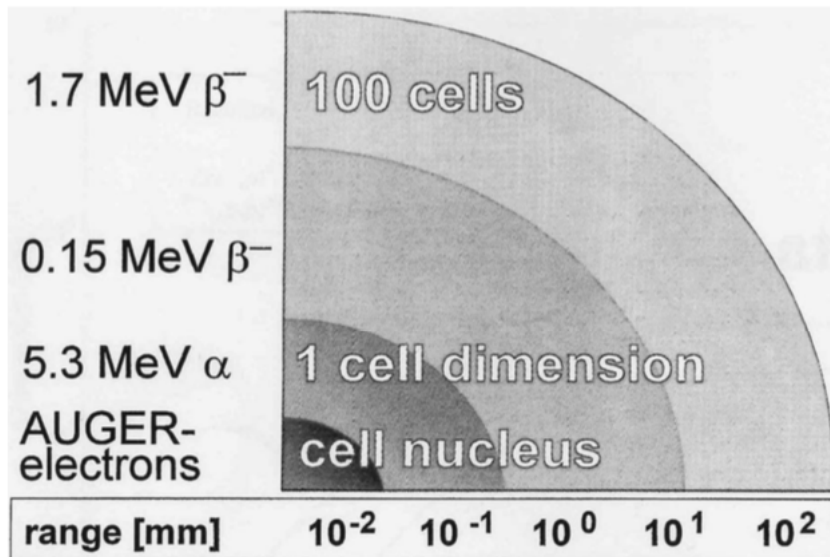


Figure 1.2: The figure illustrates the ranges of different particles on the scale of cells. Auger electrons does not exceed the cellular nucleus and alpha-particles does not exceed more than ca. 1 cell dimension which allows for very specific targeting of cells. Low energetic  $\beta^-$  emitters have ranges of ca. 1 mm. Picture is from (S M Qaim, R Capote, and F Tarkanyi. Nuclear Data for the Production of Therapeutic Ra-dionuclides. Trs 473, (473):395, 20), p. 2.

### 1.1.2 $^{193m}\text{Pt}$ as a potential therapeutic agent

$^{193m}\text{Pt}$  ( $t_{1/2}=4.33$  days) is an auger-emitting isomer which decays by isomeric transition (100%) to the long-lived  $^{193g}\text{Pt}$  groundstate ( $t_{1/2}=50$  years). Radionuclides produced from deuterons on natural iridium such as  $^{191}\text{Pt}$ ,  $^{193m}\text{Pt}$ ,  $^{192}\text{Ir}$  and  $^{194}\text{Ir}$  are believed to have potential in medicine, like chemotherapy, brachytherapy, radioimmunotherapy and imaging (Tarkanyi et.al 2006). Platinum radionuclides are of special interest, as platinum is the main element in chemotherapeutic agents such as cisplatin, which is a drug which is used clinically in treatment of testicular and ovarian cancer mainly, but also to treat esophagus, head and neck and bladder cancer<sup>1</sup>. Cisplatin (cis-dichlorodiammine platinum(II)) is an inorganic molecule which contains one stable platinum atom surrounded by two chlorine atoms and two ammonia molecules ( $\text{NH}_3$ ). The cisplatin-molecule enters the cell nucleus, and binds to the DNA, example-wise shown in figure 1.3, where the chlorine-atoms are de-attached and the platinum-atom binds through covalent bonds to the DNA base guanine (and in some cases adenine, *is that correct?*), and breaks the bonds between the DNA nitrogenous bases. Cisplatin thus targets the DNA. One of the major challenges with cisplatin is the chemical toxicity, but when auger-emitters such as  $^{193m}\text{Pt}$  or  $^{195m}\text{Pt}$  replace the stable platinum atom, the local auger-damage effect increases the chemical damage of cisplatin, suggesting that a smaller amount of the drug is required, and chemical toxicity can be avoided<sup>2</sup>.

By replacing either of the stable nitrogen atoms with the PET-radionuclide  $^{13}\text{N}$  ( $t_{1/2}=9.965$  minutes), or by a radionuclide platinum, where  $^{191}\text{Pt}$  ( $t_{1/2}=2.83$  days, decay by electron capture (100%) to  $^{191}\text{Ir}$  (stable)),  $^{193m}\text{Pt}$  and  $^{195m}\text{Pt}$  ( $t_{1/2}=4.010$  days, decay by isomer transition (100%) to  $^{195g}\text{Pt}$  (stable)) is of special interest, cisplatin can be used for imaging or therapy<sup>3</sup>, but therapy is most common.

As  $^{191}\text{Pt}$  is electron-capture emitter, can be used in imaging, with for instance 129.4 keV (38.0%) or 172.19 keV (43.2%). Combining  $^{191}\text{Pt}$  with a therapeutic agent might be possible for theranostic pair with either  $^{193m}\text{Pt}$  or  $^{195m}\text{Pt}$ ? Can be combined with therapy as it releases auger electrons?

<sup>1</sup>[https://www.sciencedirect.com/science/article/pii/S0969804399000822?casa\\_token=ZLJ8YPQzGZMAAAAAA:264QzKWpH8Kv6iHotiGMeoHTk8jKqmnoDgf709SrAD8BUWVwbRXriZbHgkYOtHg-2qyX3Hvt9E](https://www.sciencedirect.com/science/article/pii/S0969804399000822?casa_token=ZLJ8YPQzGZMAAAAAA:264QzKWpH8Kv6iHotiGMeoHTk8jKqmnoDgf709SrAD8BUWVwbRXriZbHgkYOtHg-2qyX3Hvt9E)

<sup>2</sup><http://citeseerx.ist.psu.edu/viewdoc/download?doi=10.1.1.987.2577&rep=rep1&type=pdf&page=506>, p. 493

<sup>3</sup>[https://www.sciencedirect.com/science/article/pii/S0969804399000822?casa\\_token=ZLJ8YPQzGZMAAAAAA:264QzKWpH8Kv6iHotiGMeoHTk8jKqmnoDgf709SrAD8BUWVwbRXriZbHgkYOtHg-2qyX3Hvt9E](https://www.sciencedirect.com/science/article/pii/S0969804399000822?casa_token=ZLJ8YPQzGZMAAAAAA:264QzKWpH8Kv6iHotiGMeoHTk8jKqmnoDgf709SrAD8BUWVwbRXriZbHgkYOtHg-2qyX3Hvt9E)

Decay mode: For  $^{193}\text{Pt}$ , there are three states, the isomer state at 149.8 keV, with nuclear spin  $13/2^+$  (4.33 d), a state at 14.3 keV with nuclear spin  $5/2^-$  (2.52 ns), a state at 1.6 keV with nuclear spin  $3/2^-$  (9.7 ns) and the ground state at 0.0 keV with nuclear spin  $1/2^-$  (50 y)<https://www.nndc.bnl.gov/nudat2/getdecays>. V.S. Nuclear data sheets for A=193. Nucl. Data Sheets. 32, 593-679, 1981. **here write about gamma-decay and that the probability for M6 or whatever transition is improbable.** The populated isomer states decays from 149.8 keV to 14.3 keV releasing a 135.50 keV photon (0.1145475%), from 14.3 keV to 1.6 keV releasing a 12.634 keV photon (0.70%), and from 1.6 keV to the ground state releasing a 1.642 keV photon (0.0321). The photon abundance is thus low, and this isomer is not well suited for imaging. Due to the low intensity of the gamma-rays, it might be difficult to detect. There are X-rays too, but they overlap with other nuclei. Since the gamma-rays are weak, the IC probabilities are 99.89%, 99.33% and 99.99% for each state respectively, calculated by subtracting 100 - gamma-intensity <sup>4</sup>. This also indicates that the phondon abundance is very low, as well high very high prob of low E electrons :D

In all decays, there are certain quantities in which needs to be conserved; angular momentum ( $\ell$ ) and parity (maybe  $\ell$  should be written as L instead??). Krane says that a multipole of order  $\ell$  transfers angular momentum  $\ell\hbar$  per photon (Krane, p. 333). A nuclear state has a definite angular momentum (angular momentum and spin) and parity, and if a gamma-transition is to happen between two states, the photon must connect the two states by conserving angular momentum and parity. In order for the quantity  $\ell$  to be conserved, the angular momentum can be integer values between

$$|I_i - I_f| \leq \ell \leq I_i + I_f \quad (1.10)$$

For the decay of  $^{193m}\text{Pt}$  (E level=149.8 keV) to the excited state (E level=14.3 keV), the spin and parity change is from  $13/2^+$  to  $5/2^-$ , so  $\ell = 4, 5, 6, 7, 8, 9$ . The parity decides the wether the radiation is electric multipole or magnetic multipole (equations from Krane p. 331),

$$\pi(ML) = (-1)^{\ell+1}, \quad \pi(EL) = (-1)^\ell \quad (1.11)$$

The electric decays have even parity when  $\ell=\text{even}$ , and magnetic has even when  $\ell$  is odd. If parity is unchanged in the reaction ( $\Delta\pi = \text{no}$ ), the electric multipoles are even and magnetic multipoles are odd. If the parity does change ( $\Delta\pi = \text{yes}$ ), there would be odd electric and even magnetic multipoles. Hence the possible transition from  $13/2^+$  to  $5/2^-$  are whenever  $\Delta\pi = \text{yes}$  and  $\ell = 4, 5, 6, 7, 8, 9$ , which gives possible M4, E5, M6, E7, M8 or E9.

In general, the lowest possible multipole dominates, and the emisssion of multipole of one order higher (L+1 than L), is reduced by a factor ca  $10^{-5}$  (Krane p. 335, important!!). Thus, a multipole of order 4 or 5 has a low probability of occurring and thus the isomer has a long half life. In comparison to decay from isomer state, decay from  $5/2^-$  to  $3/2^-$  gives possible radiation,  $\ell = 1, 2, 3, 4$ , with no parity change, and  $\Delta\pi = \text{no}$ , gives possible M1, E2, M3, E4, and from  $3/2^-$  to  $1/2^-$  gives  $\ell = 1, 2, 3, 4$ , which also gives M1,E2, M3, E4.

Half life: the decay rate constant is the sum of the decay rates of all the populates states transitions,  $\lambda = \lambda_{13/2^+} + \lambda_{5/2^-} + \dots$

### Gamma-decay and isomeric transition

Gamma-decay is the lowering of the excitation energy by the release of a photon, with an energy  $\Delta E$  equal to the energydifference in the two states. The typical half lives of gamma-emission are less than  $10^{-9}$  seconds, however, longer lived states of a nucleus which is not the ground state is called an isomer, and the gamma-decay of an isomer state is called isomeric transition (Krane, p. 175). Whenever gamma-decay is possible, another process called internal conversion is competing. It is an electromagnetic process, where the nucleus interacts electromagnetically with the atomic electrons, and an electron is emitted instead of the photon (Krane, chapter 10, p. 341). The kinetic energy of the emitted electron is the transition energy minus the electron binding energy

<sup>4</sup><http://citeseerx.ist.psu.edu/viewdoc/download?doi=10.1.1.987.2577rep=rep1type=pdfpage=506>, p. 496

$$T_e = \Delta E - B \quad (1.12)$$

where B is a positive number (even though bound states are negative??). The electron is called a conversion electron, and this electron is high in energy and matches the gamma-energy. The electron binding energy varies with the atomic orbital (Krane), and the electrons emitted following internal conversion are in a spectrum of different discrete energies. The transition energy must be higher than the electron binding energy, and as a consequence, the electron is labelled with the shell that it was emitted from. (remember, n=1=K, n=2=L, n=3=M, n=4=N)

In the case of the decay of  $^{193m}\text{Pt}$ , internal conversion is highly favoured instead of gamma-decay (the intensity of the gammas are very weak). The total decay probability is the summed decay probability for gamma-decay and internal conversion

$$\lambda = \lambda_\gamma + \lambda_{IC} \quad (1.13)$$

and the internal conversion coefficient  $\alpha$  can be defined as

$$\alpha = \frac{\lambda_{IC}}{\lambda_\gamma} \quad (1.14)$$

High values of  $\alpha$  indicates high probability of internal conversion, relative to probability of gamma-emission, but the coefficient diverges towards infinity when  $\lambda_\gamma$  reaches towards zero, which for instance is when the gamma-transition is zero. In general, the coefficient increases as  $Z^3$ , which will give a much greater coefficient for heavy nuclei than for lighter nuclei. In addition the coefficient decreases rapidly (ca.  $E^{-2.5}$ ) with increasing transition energy. The multipole order also affects the coefficient, where a higher multipole order indicates a higher value. For higher atomic shells than the K shell ( $n=1$ ), the coefficient decreases like  $n^{-3}$  (Krane, chapter 10, p. 346).

In therapy, the most important process is the process which occurs after the release of the conversion electron. There is a vacancy in the shell where the conversion electron was emitted, and an electron from a higher shell drops down to this energy level, with the release of an X-ray with an energy equal to the difference between the energy state of the two shells,  $\Delta E$ . If the transition is an electron from an L shell drops to K shell, and an electron from the L shell is ejected, the process is called a KLL transition, and the energy of the auger electron is  $E_{auger} = E_K - E_{LL}$  (Prasad A. Naik, in Encyclopedia of Spectroscopy and Spectrometry, 1999) <https://www.sciencedirect.com/topics/chemistry/auger-process>. If the vacancy is filled with an electron from the same shell (or subshell) but the ejected electron is from another shell, the electron is called a coster-kronig electron (like LLM, electron vacancy is moving from L to L and electron in M is emitted), and if the whole process occurs in the same shell, it is called a super coster-kronig process (MMM)

The energy of the X-rays are lower in energy than the gamma-rays, typically. If one of the X-ray photon interacts within the atomic electrons (via photoelectric effect), the electron (which is called an auger electron) will be emitted with the energy of the X-ray minus the atomic binding energy (Handbook of Nuclear chemistry, p. 390)

$$T_{a.e.} = \Delta E_{x-ray} - B \quad (1.15)$$

From the vacancy from the auger electron, a new electron can take this place and release another X-ray. The auger electron can cause further ionizations in the atom, either by interaction itself, or from X-rays following the de-excitation of another atomic electron by the vacancy. Thus it is possible to have a cascade of electrons and X-rays. The secondary electrons caused by the auger electron can lead to a cascade of new short-range electrons and X-rays, which are typically have ranges of nm in tissue (Handbook of nuclear chemistry p. 2203). Since the X-ray energy is in the low energy region, the auger electrons have low energies (from equation 1.15).

Since auger emitters are short range, they are very precise, and do only harm when bound to DNA or when incorporated into the cellular nucleus (handbook of nuclear chemistry, o. 2204), which means that no neighbouring cells will be affected.

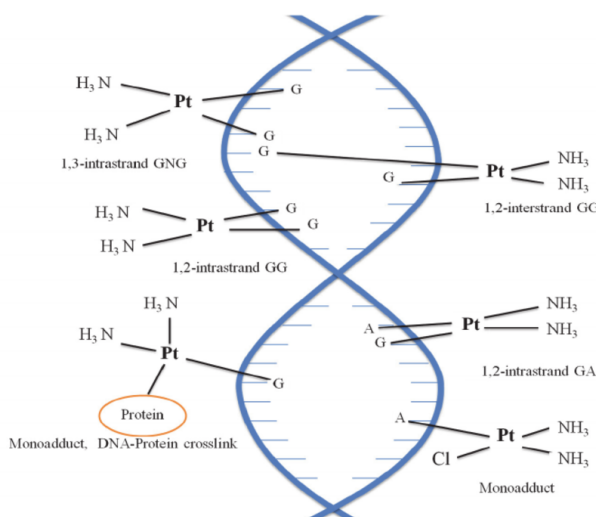


Figure 1.3: A DNA Repair Protein BRCA1 as a Potentially Molecular Target for the Anticancer Platinum Drug Cisplatin - Scientific Figure on ResearchGate. Available from: [https://www.researchgate.net/figure/Common-cisplatin-DNA-adducts-and-functions-For-instance-the-platination-of-human-serum\\_fig2\\_21919257](https://www.researchgate.net/figure/Common-cisplatin-DNA-adducts-and-functions-For-instance-the-platination-of-human-serum_fig2_21919257) [accessed 12 Apr, 2020].

After IC-process, vacancy is produced in an inner atomic shell ( $n$ ) or subshell (like  $l=spdf$ ). Vacancies in inner atomix orbitals are unstable, filled by electrons from higher energy levels. 4 processes, radiative X-ray transition, non-radiative transitions of auger, Coster-Kronig and super Coster-Kronig. move primary vacancies to higher shells or subshells. The non-radiative transitions involves multiplication of vacancies in the higher shells and subshells since two new vacancies are produced for each filled vacancy. Whenever energetically possible, super CS transitions dominate the other types. Thus the inner shell vacancies move upward to the valence and near valence shells of the atom, copious emission of electrons occur. Since the transition energies are very small for the higher shell transitions, the electrons ejected possess very small energies and is extremely short range (few nm) in biological matter, find a citation here, numb 8 in chapter.

Energy loss of low E auger electrons. In this energy region, is due to collision loss, not bremsstrahlung. Deflects frequently due to low mass, and the max energy loss is  $T_e/2$  per collision.

General stuff  $^{193m}\text{Pt}$ : Cellular nucleus is approximately  $6\mu\text{m}$ , while thickness of DNA is ca 2 nm (wikipedia). <sup>5</sup>. Range of the electrons from the decay is between 3.29nm-231 $\mu\text{m}$ , according to simulation done by Howell (1992), so well within cellular nucleus. In its decay, it emits 26.4 coster-konig and auger electrons (energy realeased per decay: 10.353 keV) and internal 3 conversion electons (energy released per decay: 126.738 keV). According to the simulation, an additative 12.345 keV is for X-ray energy deposition per decay.

Production: there are multiple ways that this isomer can be produced, either in a neutron field in a reactor, or in a charged particle accelerator like a cyclotron:  $^{192}\text{Pt}(n,\gamma)$  or via  $^{192}\text{Os}(\alpha,3n)$ . One of the issues with production is that  $193\text{m}\text{Pt}$  (and  $195\text{m}\text{Pt}$ ) are difficult to produce with high specific activity (Qaim 2016), and are not well investigated. This study gives an examination of a new route. Many reasons, reactors are on their way out, and Osmium is a poisonous and difficult target to work with, so using iridium as target is easy, (expensive though?) and the production of radionuclides below iridium is evidently in this work and in papers tarkanyi et al (2006,2019) low.

By itself, not useful for imaging.  $191\text{Pt}$  and  $195\text{m}\text{Pt}$  can. Can replace stable N with  $13\text{N}$ , but the half life is so short that the radionuclide can not image the distribution it self, so not as a theranostics pair?? or does cisplatin distribute so fast within the body?

Pt-poisoning

<sup>5</sup><https://sci-hub.tw/https://doi.org/10.1118/1.596927>

## 1.2 Radioactive decay law and Gamma-ray spectroscopy

Gamma-ray spectroscopy is a method to identify and obtain information about radioactive nuclei present in a detector. As beta and alpha decay can result in an excited daughter product, the spectrum in fact shows the de-excitation of the daughter product. Since we know that these gamma-lines are transitions which happens right after a beta or alpha decay (or isomer transition), we identify the parent with gamma-ray spectroscopy. A detector has channels in which counts are registered. These channels are ... similar to the gamma-ray energy. Thus a spectrum has channels (which increases in energy) along the x-axis and counts along the y-axis. If a detector registers many counts, it means that the state is highly populated, and the intensity of the gamma is strong (Krane, p. 351).

### 1.2.1 Radioactive decay law

From here based on Krane chapter 6<sup>6</sup>

The activity of a nucleus is defined as the number of decayed nuclei per unit time of a radioactive product, which is equal to the radioactive decay rate

$$A = \frac{dN}{dt} = -\lambda N \quad (1.16)$$

where  $N$  is the number of nuclei,  $t$  is the time and  $\lambda$  is the decay constant. Solving equation 1.16 gives number of decayed products at time  $t$

$$N(t) = N_0 e^{-\lambda t} \quad (1.17)$$

Since  $N \propto A$ , the relations  $\frac{N_0}{A_0} = \frac{N(t)}{A(t)}$  are valid, and we can rewrite the equation 1.17 to

$$A(t) = A_0 e^{-\lambda t} \quad (1.18)$$

This accounts for single nucleus decaying into a daughter product, without anything first decaying into the parent nucleus. However it is common that a radioactive nucleus decays into another radioactive nucleus. Hence the daughter activity will increase due to feeding from the parent. For multiple decay, Bateman equation is used describing the activity in nucleus  $n$  of the decay chain ([Voyles2018, which article??](#))

$$A_n = \lambda_n \sum_{i=1}^n \left[ \left( A_{i,0} \prod_{j=i}^{n-1} \lambda_j \right) \cdot \left( \sum_{j=i}^n \frac{e^{-\lambda_j t}}{\prod_{i \neq j} (\lambda_i - \lambda_j)} \right) \right] \quad (1.19)$$

where  $A_n$  is the activity of nuclei  $n$  in the decay chain, with the corresponding decay constant  $\lambda_n$ . The equation sums over all nuclei in the decay chain.  $A_{i,0}$  is the initial activity of nucleus  $i$ , and  $j$  is the nucleus which is feeding into nucleus  $i$ .

If a target of stable nuclei is assumed, which is exposed to a particle beam which induces various nuclear reactions, the constant rate of production of a specific reaction is dependent on the number of target nuclei, the current of flux of the particle beam and the reaction cross section

$$R = N_T \Phi \sigma \quad (1.20)$$

where  $R$  is the production rate,  $N_T$  is the number of target nuclei,  $\Phi$  is the beam current or flux and  $\sigma$  is the reaction cross section. In the assumption of the production rate being a constant value, the number of transformed target nuclei is small in comparison to the total number during the irradiation time. The number of produced nuclei from a specific reaction per unit time is thus the produced nuclei minus the decayed nuclei (activity)

$$dN = R dt - \lambda N dt \quad (1.21)$$

which has the solution

---

<sup>6</sup><https://faculty.kfupm.edu.sa/phys/aanaqvi/Krane-Ch-6.pdf>

$$N(t) = \frac{R}{\lambda}(1 - e^{-\lambda t}) \quad (1.22)$$

From equation 1.16, the total activity produced during irradiation time  $t$  is thus

$$A(t) = R(1 - e^{-\lambda t}) = N_T \Phi \sigma (1 - e^{-\lambda t}) \quad (1.23)$$

At the end of beam, the activity is denoted as  $A_0$ , and  $t$  is the irradiation time:

$$A_0 = N_T \Phi \sigma (1 - e^{-\lambda \Delta t_{\text{irr}}}) \quad (1.24)$$

When a target is irradiated, the activity of the product nucleus will increase until secular equilibrium is achieved, which is when the product rate and decay rate are constant. Hence it is not necessary to irradiate a target for more than 2-3 half lives.

If a spectrum is counted at a delay time  $\Delta t_d$  after end of beam with a counting time  $\Delta t_c$  the total number of decayed products are

$$N_D = \int_{\Delta t_d}^{\Delta t_d + \Delta t_c} A(t) dt \quad (1.25)$$

Using equation 1.18 for  $A(t)$ , the solution to the above equation is

$$N_D = \frac{A_0}{\lambda} e^{-\lambda \Delta t_d} (1 - e^{-\lambda \Delta t_c}) \quad (1.26)$$

which again is equal to

$$N_D = \frac{A(t)}{\lambda} (1 - e^{-\lambda \Delta t_c}) \quad (1.27)$$

We can only know the number of decayed products which are detected. This is dependent on the efficiency of the detector, the intensity of the gamma-rays and the true number of decayed products

$$N_C = N_D \epsilon I_\gamma \quad (1.28)$$

where  $N_C$  is the number of observed/collected gamma-rays,  $\epsilon$  is the efficiency of the detector and  $I_\gamma$  is the gamma-ray intensity.

Thus, we can obtain an expression for  $A(t)$  after a delay time:

$$A(t) = \frac{N_C \lambda}{\epsilon I_\gamma (1 - e^{-\lambda \Delta t_c})} \quad (1.29)$$

Again using 1.18 for  $A(t)$ , the above expression can be rewritten using  $A_0$  and the delay time  $\Delta t_d$

$$A_0 = \frac{N_C \lambda}{\epsilon I_\gamma (1 - e^{-\lambda \Delta t_c}) e^{-\lambda \Delta t_d}} \quad (1.30)$$

### 1.2.2 High purity Germanium detector

High purity Germanium detector is a type of semiconductor, which is a material where the energy required to remove an electron from the valence band (in the outer atomic shell) to the conduction band is small. The germanium atom has atomic number 32, and 4 valence electrons in the outer p4 shell (need citation?). The atoms in the detector are bound through covalent bonds in a crystal structure. The main mechanism of a semiconductor is creation of electron-hole pairs after energy deposition of an ionizing particle in the crystal. If an electron is excited to the conduction band, a hole is left. This hole can move as a neighboring electron fills this spot, and it can cause a chain reaction, and the hole will move in the crystal. Both the electron in the conduction band and the hole in the valence band contributes to an electric current. Under influence of an electric field, the electron-hole pairs will be collected and we can measure the incident as a count. The major

advantage with semiconductor detector is that the average energy to create an electron-hole pair is very low, which results in a superior energy resolution in comparison to other detectors like gas and scintillation detectors. High energy resolution advantageous in gamma-ray spectroscopy which makes it possible to separate gamma-ray peaks within less than a keV. At room temperature, thermal energy can excite the electron from the valence to the conduction band and cause noise in spectra. Therefore, Germanium detectors are operated at 0 Kelvin. Write about recombination and trapping, noise, np semiconductor junction, depletion depth?? (Techniques for Nuclear and Particle Physics Experiments, William R. Leo, p. 215-216).

Ideally, for all gamma-rays with the same energy, should be detected in the same channel giving a step function. However, realistically, the resolution of a detector is not that good, and instead of seeing a delta peak, the peak is typically gaussian shape with a finite width. The full width half maximum  $\Delta E$  of the peak tells us how well the relative resolution at gamma-energy  $E$ ,

$$\text{resolution} = \frac{\Delta E}{E} \quad (1.31)$$

The energy resolution is important, as it tells us how well it can distinguish two close lying peaks from each other (Techniques of Nuclear and particle Physics.. , p. 117). The resolution of a germanium detector very good (0.1% for a 1 MeV gamma-ray) in comparison to for instance NaI detector (8-9% for a 1 MeV gamma-ray) (Techniques of Nuclear and particle Physics.. , p. 117). **explain why, prob in semiconductor chapter!**

The peak itself is not directly gaussian. Ionizing radiation statistics is based upon Poisson statistics, where the probability of observing  $N$  events is a discrete value

$$P(N) = \frac{\mu^N e^{-\mu}}{N!} \quad (1.32)$$

where  $\mu$  is the mean value. This distribution counts when the probability is a small (eg decay prob?) value and that the total number of trials are large (number of decays) (Techniques of Nuclear and particle Physics.. , p. 85). For poisson distribution, the average is equal to the variance;  $\sigma^2 = \mu$ . From there, the standard deviation ( $\sigma$ ) is thus equal to the square root of the average.

The distribution is not symmetric, but as  $\mu$  increases in value, the peak approxes a gaussian shape. The total number of counts is the area of the peak. The total peak is a Gaussian assumption but with an exponential skew towards low  $E$  caused by incomplete charge collection, and a step function for taking compton background into account.

In calculation of the peak area, there are two uncertainties of relevance, the relative statistical uncertainty in the counting from the Poisson statistics,

$$\sigma N_i = \sqrt{N_i} \quad (1.33)$$

If number of counts  $N_i = 10000$ , the relative uncertainty ( $\frac{\sigma N_i}{N_i} = \frac{1}{\sqrt{N_i}} = 1\%$ ). Therefore we say that a good number of counts is 10000 or more to reduce the statistical uncertainty. The other is systematic in the detector, and can for instance be due to a process called annealing, which is heat damage to the detector. Can fix by taking a blanket of resistor wrap crystal in, rise to high temp, let it sit and slowly deheat to room temp, traps will diffuse and detector is repaired (this is notes from Andrew).

Also write about deadtime!

### 1.2.3 Gamma-ray spectrum

Spectrum: consists of photopeaks, a compton continuum, compton edge, backscatter peak, single escape double escape. In cases where positrons exist, chances of having a broad fat 511 keV peak.

Germanium detectors, highest resolution for gamma-rays, from few keV to 10 MeV. The peak to Compton ratio is much greater due to the higher photoelectric cross section of Germanium . The largest challenges are with signal to noise ratio, it is important to shield very well to minimize background radiation (Techniques for Nuclear and particle..... William R. Leo, p. 241).

here from another citation: "Practical Gamma-ray Spectroscopy". Gordon R. Gilmore. Nuclear Training Services Ltd Warrington UK. (can be find under articles in masterthesis). This book can also be used in particle interaction in matter check!! In a detector, the particles interacts as the photons described in particle interaction, via photoelectric, compton scattering and pair production. Photoelectric absorption where the photon is completely absorbed by atomic electron is desired because all of the energy is deposited within the detector. For a compton scattering event, if the resulting photon's energy is also deposited in the detector (for a large detector), then the total energy would add up. Same for pair production. The photon must interact in the detector volume, and the resulting electron and positron energy is deposited in the detector volume. However when the positron slows down, it annihilates with one atomic electron, releasing two 511 keV photons. If both annihilation photons's energy is deposited in the detector volume this will also contribute to a full width peak. If one 511 photon escape and the other is deposited, there will be a peak at  $E_{\gamma} - 511$  keV, and if both peaks escape, there will a double escape peak at  $E_{\gamma} - 1022$  keV. The "degree of incomplete absorption" depends upon the size of the detector and the gamma-ray energy. As previously discussed photoelectric effect dominates at low energies, and the less compton scattering and of course pair production (for E gamma higher than the threshold.). The detector size also matters because the larger the more room for the photon to scatter in and lose energy before escaping. (p. 32)

The total spectrum can be seen on p. 33 in the book. Pile-up is done because of random summing, determined by the statistical probability of two gamma-rays being detected at the same time and therefore on the sample count rate.

Interaction with detector shielding: Photoelectric effect can be followed by emission of characteristic X-ray of the absorbing medium. X ray can escape the shielding and be detected by the detector. Compton scattering: most gamma rays are scattered through a large angle by the shielding, BACKSCATTERED. Whatever the initial energy was (if scattered by more than 120 degrees) are within 200-300 keV. Peak appears as broad. Pair production: annihilation peak (511 peak) caused by the escape of one of the 511 keV photons from the shielding following annihilation of the pair production positron. Analogous to the single and double escape mechanisms within the detector but only on 511 keV photons can ever be detected since they are emitted in the opposite direction. So in order to have a 511 peak, energy of gamma ray must be more than 1022 keV. (p. 34-35).

The 511 peak can also be expected when positron emitters are present since beta + particle interacts with electron.

Since Compton scattering can be in a spectrum of energies, the gives rise to a Compton continuum, before the gamma-ray escapes the detector.

The shape of the peak: The peak is a histogram that approximate a Gauss curve (p. 186). Peak searching (SAMPO) using first and second order derivatives to search for peaks (p.185) Due to incomplete charge collection (that electron or holes are not collected) no matter how caused moves counts from the centre of the Gaussian distribution to lower channels, creating a low energy tail to the peak (p.135).

**Include a picture of peak shape and gamma-ray spectrum!! from the same book**

## 1.3 General nuclear reaction theory

**paragraph based on special curriculum** Medical radionuclides can be produced directly using charge particle (cyclotron) or neutron beams (reactors), or indirectly using radionuclide generators or fission (reactor). Medical radionuclides are typically produced in reactors, cyclotrons or by a longer lived-parent decaying into a short-lived daughter in a radionuclide generator system. In general, the production should be cheap, available. Today many radionuclides are only produced in reactors, which is the main source of neutrons, and with reactors aging (Chai Hong Yeong, Mu hua Cheng, and Kwan Hoong Ng. Therapeutic radionuclides in nuclear medicine: Current and future prospects. Journal of Zhejiang University: Science B, 15(10):845–863, 2014.), we need alternative routes to produce critical

radionuclides. Cyclotrons have many benefits, like size so that it can be produced directly at the site of usage. One of the major disadvantages is that there is a need to enriched targets to get the desired reaction, and those can be very expensive. Along with high beam intensity the melting of the target can give challenges, so target cooling techniqueis need to be there.

In order to create isotopes, nuclear reactions need to occur. There are many different production routes available for a single radionuclide, which is dependent on multiple factors such as choice of target, incident particle-beam and beam energy. To each reaction route, there is an corresponding excitation function which tells us how probable the reaction channel is at various energies. The nuclear reaction data is very important for the optimization of the product, achieving minimal level of isotopic impurities and maximum yield (S M Qaim, R Capote, and F Tarkanyi. Nuclear Data for the Production of Therapeutic Radionuclides. Trs 473, (473):395, 2011., p. 3).

Isotopic purity is important as it is impossible to separate isotopes of the same element (Syed M. Qaim. Nuclear data for production and medical application of radionuclides: Present status and future needs. Nuclear Medicine and Biology, 44:31–49, jan 2017.). An undesired radionuclidel can lead to undesired dose to healthy tissue, and a non-radioactive nuclide may lead to poisoning (if large amounts injected), but it will not have any therapautic effect. This is especially important when working with poisoeneos elements such as platinum. The only option to minimize isotopic impurities is to choose an appropriate energy window.

Using charged particles instead of neutrons allows for measurement at multiple energies as the particle energy degrades in the foils. The neutron energy is not degraded in the same way, due to electric neutrality, thus can only give cross section at one single energy.

### 1.3.1 Nuclear reactions and reaction cross sections

A nuclear reaction in the energy ranges of isotope production via the Compound nucleus conserves quantities such as mass-energy, linear momentum, the total number of nucleons, angular momentum and parity [cite, Krane?](#). A nuclear reaction is denoted as

$$X(a, b)Y \tag{1.34}$$

where X is the target, a is the incoming projectile, b is the outgoing decay channel and Y is the product of the nuclear reaction (Krane, chapter 11.1). There are multiple processes which can occur, radiative capture is the process where a particle is captured and a  $\gamma$ -ray is emitted in a  $(x, \gamma)$  process. If the incoming and outgoing particle is the same, it is a scattering process, where elastic scattering leaves the target nucleus in the energy same state, and inelastic if the target nucleus is in an excited state. In these type of experiments however, we are interested in emission of particles to create products in which we can measure the reaction cross section.

The cross section for a reaction can be divided into the cross section of the formation of the compound nucleus via interaction with the incoming projectile a, and the probability that the compound nucleus decay by decay channel b. The total reaction cross section is thus the sum of all the different reaction channels,

$$\sigma = \sum_b \sigma(a, b) \tag{1.35}$$

where b can be multiple particles. The general equation which is used to calculate cross sections in this experiment is the following equation

$$\sigma(E) = \frac{A_0 \cdot t_{\text{irr}}}{N_T \cdot \Phi(E)(1 - e^{-\lambda t_{\text{irr}}})} \tag{1.36}$$

where  $A_0$  is the end of beam activity of the resulting product nucleus (Y),  $t_{\text{irr}}$  is the irradiation time,  $N_T$  is the number of target nuclei (X),  $\Phi(E)$  is the projectile flux (a), and  $\lambda$  is the decay constant of the product nucleus.

The compound nucleus model (Bohr, 1936) is a model which describes the formation of a compound nucleus by absorption of an incoming projectile by a nucleus close enough to interact with the strong nuclear force, and the decay of the compound nucleus. The kinetic energy shared between the incoming projectile and the nucleon which was struck leads to multiple collisions with other nucleons and rapid exchange of energy. The energy is distributed throughout the nucleus, leaving the original nucleus in an highly excited state. The average energy per nucleon is not sufficient to overcome the binding energy of the nucleus, but due to the statistical distribution in energies there is a probability that one or more nucleons may get sufficient energy to escape the nuclear potential (Krane, chapter 11.10, p. 416). This is decay of the compound nucleus, and this will lower the excitation energy. We can include the formation of the compound nucleus in the nuclear reaction as



where  $C^*$  is the excited compound nucleus (Krane, chapter 11.10, p. 416)

For each possible decay channel of the compound nucleus, there is an associated probability or cross section, which is dependent on the energy of the incoming projectile. A function which evaluates the various cross sections at different energies is called an excitation function. In figure 1.4, the excitation function of the reactions channels for the platinum isotopes  $^{188,189,191,193m}\text{Pt}$  resulting from deuterons on natural iridium is plotted. The nuclear chart for these reaction channels can be seen in figure 1.5. Natural iridium consists of two stable isotopes,  $^{191}\text{Ir}$  (37.3% abundance) and  $^{193}\text{Ir}$  (62.7% abundance).  $^{193m}\text{Pt}$  can only be produced from  $^{193}\text{Ir}$ , ejecting 2 neutrons in the process, which can be denoted as  $^{193}\text{Ir}(\text{d},2\text{n})^{193m}\text{Pt}$  ( $^{193}\text{Pt}$  is the compound nucleus formation of deuteron on  $^{191}\text{Ir}$ , which has a low production cross section). The other platinum isotopes can be produced as  $^{191}\text{Ir}(\text{d},2\text{n})^{191}\text{Pt}$  or  $^{193}\text{Ir}(\text{d},4\text{n})^{191}\text{Pt}$ ,  $^{191}\text{Ir}(\text{d},4\text{n})^{189}\text{Pt}$  or  $^{193}\text{Ir}(\text{d},6\text{n})^{189}\text{Pt}$  and  $^{191}\text{Ir}(\text{d},5\text{n})^{188}\text{Pt}$  or  $^{193}\text{Ir}(\text{d},7\text{n})^{188}\text{Pt}$ . For each reaction route possible, there is a local maxima for the specific route **what is the edges on 188, 189 and 191Pt?**. Hence,  $^{193m}\text{Pt}$  has only one maxima, and the other platinum isotopes has two. The desired particle emission is energy dependent, and the higher energy given to the compound nucleus, the probability that more particles will be emitted is higher (Krane, chapter 11.10, p. 419). When a specific isotope is desired, the excitation function can tell us which energy window that maximizes the production and most importantly minimizes particularly other isotopes of the same element, due to the difficulty of separating same chemical elements.

### 1.3.2 Energetic factors in nuclear reactions

The nucleus is bound together by the strong nuclear force in the nuclear potential well, with a radius up to a few femtometer. The nuclear potential can be illustrated in figure 1.6, denoted as *nuclear potential*. The Coulomb barrier is a repulsive barrier for charged particles. For a charged particle induced nuclear reaction, the energy should exceed to potential, or there will be an elastic scatter. However, there is a chance of tunneling, which drops with a factor  $1/r$  where  $r$  is the distance from the center of the nucleus (Handbook of Nuclear Chemistry, chapter 3 - Nuclear Reactions, section, 3.2.3). The barrier also constraints the emission of particles for a decay channel of the compound nucleus, as the energy for an outgoing decay channel of positive particles must exceed the barrier. There is also a centrifugal barrier, which is dependent on the orbital angular momentum of the the nucleus. The orbital angular momentum is dependent on the mass and energy of the particle, but also the impact parameter of the reaction, which is the "distance" between the projectile and the nucleus

$$\ell\hbar = (mv)b, \quad b \leq r_a + r_X \quad (1.38)$$

where  $r_a$  and  $r_X$  are the radii of projectile and target nucleus. If  $\ell = 0$ , the impact parameter is zero. If  $\ell \neq 0$ , then some of the energy of the projectile will go to rotational energy of the nucleus (Handbook of Nuclear Chemistry, chapter 3 - Nuclear Reactions, section, 3.2.4). The probability of this drops with  $1/r^2$ , and if the impact parameter is large, this will constraint some of the energy that would have gone to the nuclear reaction. Figure 1.6 shows an overview of the various potentials;

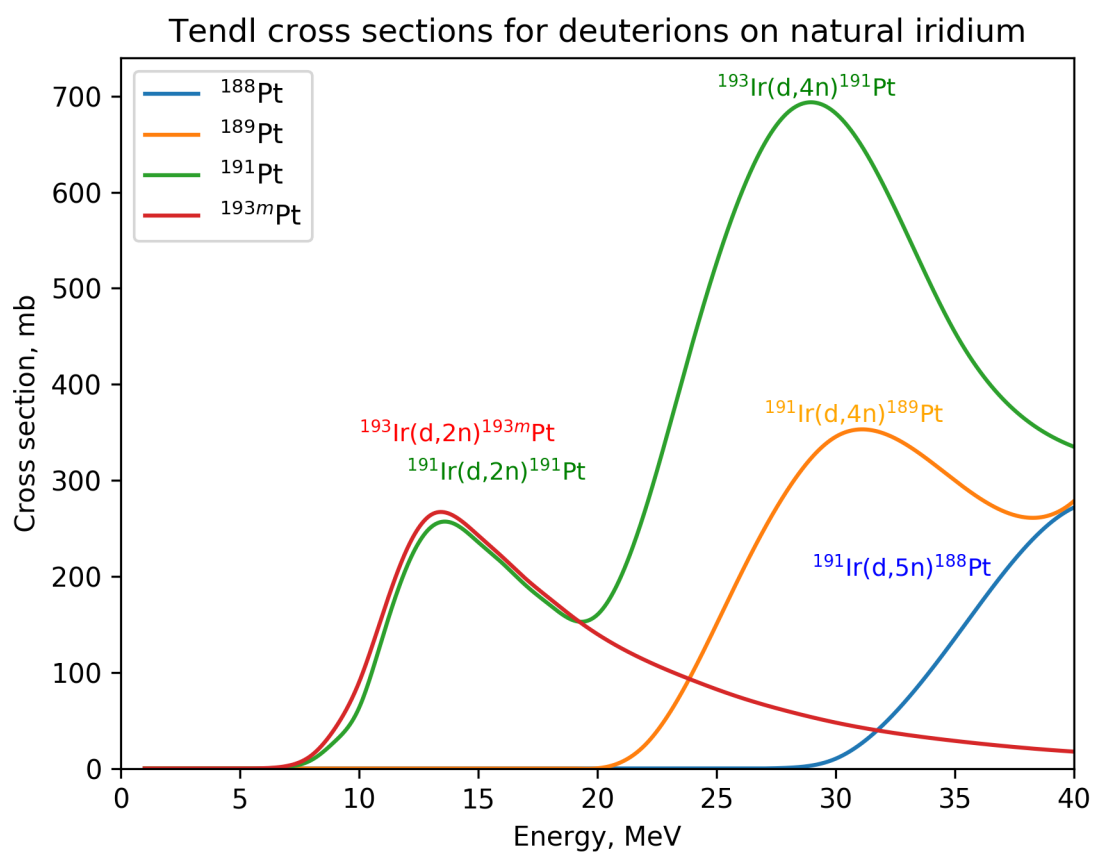


Figure 1.4: Reaction cross sections provided by Tendl for the reactions  ${}^{\text{nat}}\text{Ir}(d,x)^{188,189,191,193m}\text{Pt}$



Figure 1.5: Nuclear chart for the platinum isotopes which can be produced from natural iridium

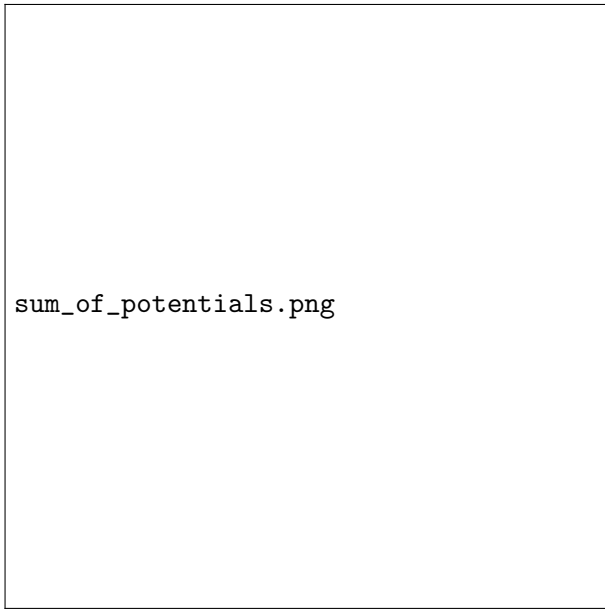


Figure 1.6: The figure shows the nuclear potential well for the strong nuclear force, along with the Coulomb repulsion barrier and the centrifugal barrier for  $^{58}\text{Zn}$ . The figure is only meant as an illustration. <https://www.researchgate.net/figure/The-RMF-potential-energy-sum-of-the-scalar-and-vector-potentials-for-the-nucleus-58-30fig6257811951>

centrifugal barrier, Coulomb barrier and nuclear potential. The figure is for  $^{58}\text{Zn}$ , but the figure is only an example. **maybe make figure self?**.

In a nuclear reaction, the mass-energy is conserved, which is denoted as the Q-value. The reaction Q-value is the difference in masses between before and after the nuclear reaction occurred (Krane, chapter 11.2). It is defined as

$$Q = (m_i - m_f)c^2 = (m_X + m_a - m_Y - m_b)c^2 \quad (1.39)$$

where  $m_i$  is the initial mass,  $m_f$  is the final mass and  $c$  is the speed of light. If  $Q > 0$ , then the reaction is exoergic, which means that energy is released in the reaction. There is no threshold energy of the projectile required for the reaction to occur, if only the projectile is present the reaction can occur. If  $Q < 0$ , then the reaction is endoergic, which means that the kinetic energy of the incoming projectile is converted into nuclear mass or binding energy. For endoergic reactions to occur, there is a minimum threshold energy of the projectile in order for the reaction to happen, which is defined as (Krane, 11.2, p. 382)

$$E_{\text{threshold}} = (-Q) \cdot \frac{m_Y + m_b}{m_Y + m_b - m_a} \quad (1.40)$$

The energy threshold thus depend on the Q-value, the Coulomb barrier for charged particles, and the centrifugal barrier if angular momentum  $\ell \neq 0$ . The parity though depend, even numbers of  $\ell$  mix with even, and odd with odd (Handbook of Nuclear Chemistry, chapter 3Nuclear Reactions, section, 3.2.3). This gives an indication on when a reaction can energetically occur, but does not tell us how probable the reaction is. Equation 1.40 indicates that a higher mass for the particle in the outgoing channel  $m_b$ , will lower the energy threshold.

The nuclear binding energy is a number which tells us how tightly bound the nucleus is, and much energy is required to separate nucleons from the nucleus. The nuclear binding energy is related to the mass of the nucleus, through the famous equation

$$E = mc^2 \quad (1.41)$$

The binding energy is the mass-difference between the nucleus as a whole, and the number of protons and neutrons added

$$B = c^2(z \cdot m_p + n \cdot m_n - m_N) \quad (1.42)$$

where  $z$  is the number of protons,  $n$  is the number of neutrons,  $m_p$  is the proton mass,  $m_n$  is the neutron mass,  $M_N$  is the mass of the nuclide, which is the number of nucleons  $A$  minus the number of electrons,  $M_P = m_A - z \cdot m_e$  (the electronic binding energy per electron is excluded). From Krane's derivation of the nuclear binding energy (Krane, chapter 3.3, p. 65), the equal number of protons and neutrons make up  $z \cdot {}^1H$ , thus we can rewrite equation 1.42 to

$$B = z \cdot m_{}H + n \cdot m_n - m_A \quad (1.43)$$

Separation energy of a particle is the energy required to be removed from the nucleus. This is defined as the difference in binding energy between the nucleus with the particle and the nucleus without the emitted particle. Since heavier particles such as tritium has a lower binding energy, more energetically easy to separate.  $n$  and  $p$  require more.

Write about the semi-empirical mass formula, and what terms that affects the decay of compound. Especially the parity term? Odd A or even A. If A odd, decay by proton, since then A is even. If A is even, then decay by alpha for A to remain even. But why is n,p favoured over for instance t??

### 1.3.3 Nuclear cross sections

The cross section for a reaction can be divided into the cross section of the formation of the compound nucleus via interaction with the incoming projectile  $a$ , and the probability that the compound nucleus decay by decay channel  $b$ . The total reaction cross section is thus the sum of all the different reaction channels,

$$\sigma = \sum_b \sigma(a, b) \quad (1.44)$$

where  $b$  can be multiple particles. The general equation which is used to calculate cross sections in this experiment is the following equation, which is solved from equation 1.24 (referenced to in the later parts of the paper)

$$\sigma(E) = \frac{A_0}{N_T \Phi(E) (1 - e^{-\lambda \Delta t_{\text{irr}}})} \quad (1.45)$$

not, need to check if this is the correct one..

$$\sigma(E) = \frac{A_0 \cdot t_{\text{irr}}}{N_T \cdot \Phi(E) (1 - e^{-\lambda t_{\text{irr}}})} \quad (1.46)$$

where  $A_0$  is the end of beam activity of the resulting product nucleus ( $Y$ ),  $t_{\text{irr}}$  is the irradiation time,  $N_T$  is the number of target nuclei ( $X$ ),  $\Phi(E)$  is the projectile flux ( $a$ ), and  $\lambda$  is the decay constant of the product nucleus.

Why we are interested, why is there a need for nuclear production cross sections.

The Q-value for nuclear reactions

Compound nucleus, what happens. Q value, binding energy, particle emission, probabilities (why does n, p/alpha emission require higher energy, but is more favoured than T emission if both possible.)

### 1.3.4 Expected products from deuterions on iridium, iron, copper and nc

Include figure of different nuclear charts, and write about Q values, and reaction channels, which makes it more probable that we observe it (eg. when neutron, proton/alpha channels opens).

## 1.4 From book

In a nuclear reaction, the energy, linear momentum, the total number of protons and neutrons, angular momentum and conservation of parity is conserved.

The compound nucleus; the collisions are described by a model called Multistep Compound Model (Feshback, Kerman and Koonin, 1980), which is the model that reaction modeling code EMPIRE and TALYS rely on. **find out what ALICE does ???**

Products of a nuclear reaction can be anything than conserve the various variables. Mass energy conservation is the Q-value, which is the mass difference in the reactant nuclei (projectile and target in this case) and product nuclei (decay channel particles and product). Binding energy (nuclear mass energy) often denoted as  $\Delta = (M_0 - Au)c^2$ , where A is atomic mass number, u is atomic mass unit. Q-value can be rewritten:

$$Q = \Delta_{\text{projectile}} + \Delta_{\text{target}} - \sum \Delta_{\text{products}} \quad (1.47)$$

Charged particle reactions with heavy nuclei which is the case here, can have positive or negative Q-value. If the Q-value is negative, energy is required to induce the reaction. The reaction is negative if the sum of products is less than the sum of reactants. The excitation energy of the product nucleus is the extra energy which is deposited in the product nucleus. The decay of this is often times  $\gamma$ -rays (?). If the excitation energy is lower than the binding energy of the nucleus? Threshold is the minimum energy required for the incoming projectile to form a product nucleus, which is then in its ground state.

$$\text{mass-energy : } \Delta_t + \Delta_p + E_p \quad (1.48)$$

## 1.5 The decay of the compound nucleus

At the energy ranges in which this work is operating in, the nuclear reaction is caused by a fusion between the incoming projectile to create an highly excited compound nucleus.

The decay favoured decay channel is dependent on multiple properties such as the charge and angular momentum. The coulomb potential is defined as

$$U_c = K \frac{z_1 z_2 e^2}{A_1^{1/3} + A_2^{1/3}} \quad (1.49)$$

where z is the the number of charges, e is the electrical charge and  $A^{1/3}$  is the nuclear radius which is equal to  $r = r_0 A^{1/3}$ . K is a constant value.

The centrifugal barrier (which is the amount of energy which is conserved in rotational energy) depends on the angular momentum

$$U_s = \frac{\hbar \ell (\ell + 1)}{2 \mu r^2} \quad (1.50)$$

where  $\mu$  is the reduced mass  $u \cdot \frac{A_1 A_2}{A_1 + A_2}$ .

Table 1.1: The table shows the most common decay channels for the decay routes available in this energy region.  $\Delta$  is the binding energy of the alpha particle, which can be calculated using equation 1.42, where the mass of the proton is  $m_p = 938.28 \text{ MeV}/c^2$  and  $m_n = 939.57 \text{ MeV}/c^2$ .  $\Delta$  is thus the difference in energy-mass between the particle composed of protons and or neutrons, and a equal number of protons and neutrons independent. All parities are positive due to angular momentum  $\ell = 0$ .

Particle	$\Delta(\text{MeV})$	$J^\pi$	Charge
p	-	$\frac{1}{2}^+$	+1
n	-	$\frac{1}{2}^+$	0
d	2.2	$1^+$	+1
t	8.5	$\frac{1}{2}^+$	+1
${}^3\text{He}$	7.7	$\frac{1}{2}^+$	+2
$\alpha$	28.3	$0^+$	+2

Target	Proton	neutron	deuteron	triton	${}^3\text{H}$	$\alpha$
Fe (Z=26)						
Ni (Z=28)						
Cu (Z=29)						
Ir (Z=30)						

Table 1.2: The Coulomb barrier in MeV for each of the targets. Can be used to explain why we see what we see.

Table 1.1 might be wrong in the sense  $J^\pi$ . Might just be the total spin which is of interest? But since  $J = l + s$ , the spin will give a higher intrinsic angular momentum. Since  $|I_i - I_f| \leq \ell \neq I_i + I_f$ ,  $\ell$  can be multiple values, and the parity is thus dependent on the value here. (Krane, chapter 8.5, p. 257). The centrifugal potential is thus

$$U_{0,s} = \frac{\ell(\ell+1)\hbar}{2mr^2} \quad (1.51)$$

and the Coulomb potential is

$$U_{0,c} = K \frac{z_1 z_2 e^2}{A_1^{1/3} + A_2^{1/3}} \quad (1.52)$$

The

The total angular momentum  $J$  is the sum of the orbital and intrinsic angular momentum (spin), thus

$$\mathbf{J} = \ell + \mathbf{s} \quad (1.53)$$

The spin is the sum of unpaired paired protons and neutrons. The total nuclear spin is thus  $I = \sum_i J_i$ . The value of the angular momentum is

$$|I_i - I_f| \leq \ell \geq |I_i + I_f| \quad (1.54)$$

Thus,



# Chapter 2

## Experimental setup

### 2.1 Lawrence Berkeley National Laboratory's 88" Cyclotron

Lawrence Berkeley National Laboratory (LBNL) is a national research laboratory on behalf of the U.S. Department of Energy through its Office of Science, and is operated by University of California, Berkeley. LBNL was founded by Ernest Orlando Lawrence, the inventor of the cyclotron <sup>1</sup>.

The 88" Cyclotron has many purposes, and can accelerate both light and heavy ions up to Uranium, with a cyclotron number  $K=140$  <sup>2</sup>. The cyclotron number is the maximum kinetic energy which can be reached for protons (with no relativistic factors taken into account). The maximum kinetic energy a particle can gain is found from the cyclotron number:

$$\frac{E_k}{A} = K \left( \frac{Q}{A} \right)^2 \quad (2.1)$$

For deuterons with mass number  $A=2$  and charge  $Q=1$ , the maximum kinetic energy is  $E_k = 70$  MeV. There are multiple programs that takes place in the facility; chip testing and space effects testing, super heavy element searches, fundamental nuclear structure measurements, novel scintillation characterization, fission yield and neutron inelastic scattering measurements (GENESIS) (from Andrew). Medically motivated isotope production goes under fundamental nuclear structure experiments.

A cyclotron is a device that accelerates positively charged particles. It is operated by an alternating electric field, and a perpendicular magnetic field, which by the Lorentz Force forces the particle to accelerate in an outward spiral. The facility is figured in figure 2.1, which consists of a cyclotron vault, and experimental caves in which the beam can be bent to with bending magnets. Faraday cups (not in figure) can measure the beam current at different steps along the tube, which makes it possible to measure the transition efficiency of the beam. Faraday cups are dense metal block, usually 6-7 cm broad Copper and Tantilum. It works as a beam stopper, and can be lowered into the beam line to measure the current. It is electrically isolated, which makes it possible to measure the current, since we know the number of initial particles accelerated. Due to electrons close to surface might be scattered off, it can read off higher positive charge than what is correct. Therefor, a magnet surrounds the cup to bend the electrons back to the Faraday cup in what is called magnetic suppression. Cave 0 is used mainly for neutron beam, chemistry, and isotope production, and was used for irradiation of the target stack.

### 2.2 The experiment

The main motivation of this experiment was to measure cross sections of the products produced after irradiation of a stack of thin Nickel, Iridium, Copper and Iron foils, with a 33 MeV incident deuteron beam, as shown in figure 2.2.

---

<sup>1</sup><https://www.lbl.gov/about/>

<sup>2</sup><http://cyclotron.lbl.gov/home>

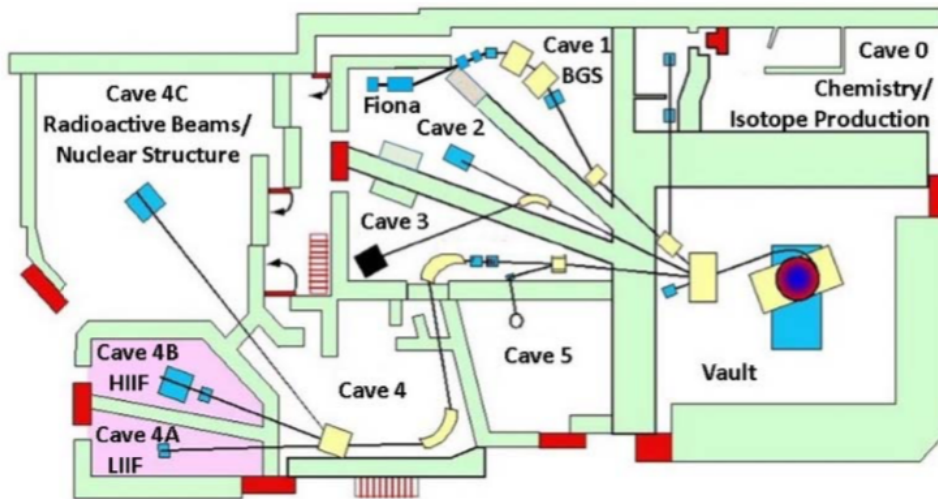


Figure 2.1: An overview of the 88" Cyclotron facility. <https://cpb-us-e1.wpmucdn.com/sites.usc.edu/dist/7/89/files/2018/04/133-18q03um.pdf>

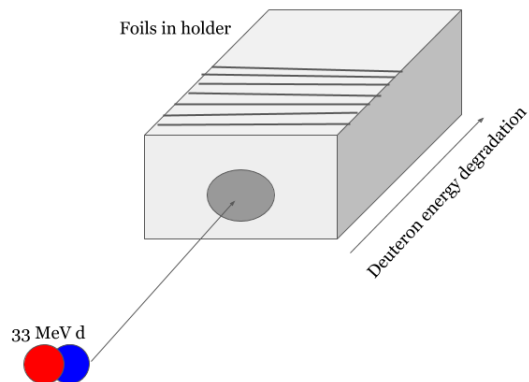


Figure 2.2: The fundamental idea of the experiment where a stack of targets are placed in a target holder, and irradiated with accelerated 33 MeV deuterons. As the energy degrades through the beam stack, it is possible to have multiple cross section measurements at different energies.

The beam was ca. 1 cm in diameter, and with each target foil being ca. 25 by 25 mm, the beam was underfilled. As the energy was degraded through the stack, multiple cross sections at different energies were possible to measure for the different induced reactions. For production cross section data experiments, thin targets (foils) are used, in the other of a few  $\mu\text{m}^3$  are used, since the induced activity is low, meaning that the deadtime of the detector and the dose to human will be low. Equation 1.45 is the equation which is used in the calculation of the cross sections. The end of beam activity goes into the equation, which is given in equation 1.29. The activity from spectra measured at different delay times after end of beam can be found, with respect to number of counts, efficiency of detector, intensity of gamma-rays, the decay constant of the nucleus  $\lambda$  and the counting time  $\Delta t_c$ . As we know that radioactive decay curves follows equation 1.19, and dependent on how many step the decaychain consists of, the end of beam activity can be estimated by extrapolating backwards in time with a curve fit.

In order to calculate the cross section of a product, end of beam activity, number of target nuclei and beam current must be found, where for the end of beam activity, the detector efficiency need to be estimated. The nickel, copper and iron deuteron-induced cross section are well-established, and can be used to determine the beam current throughout the stack.

### 2.2.1 Target design and foil characterization

A stack of ten natural iridium foils (99.9%), ten natural nickel foils (..%), ten natural copper foils (..%) and three natural iron foils (..%), along with two stainless steel foils in the front and the back of the stack, a proton degrader (a 6061 aluminum alloy), along with one extra nickel neutron monitor foil. The order of the stack can be seen in table 2.1.

Each foil were cut into approximately 25 by 25 mm squares, and each foil was characterized using a caliper to measure the length across each side, a gauge caliper to measure the thickness and a weight to measure the mass of each foil which was prewashed with isopropanol. For each measurement, the unit was measured 4 times, and the values states in table 2.1 are averaged values. The length and mass were used to measure the mass density. The thickness was not used in the calculation of the mass density, but was a good indication that the foil thicknesses were more or less consistent. **For underfilled beams, the mass density of the foil is used to find the number of nuclei per  $\text{cm}^2$ , by using the area of each foil.** The mass density was calculated using the mass of each foil divided by the area

$$\rho\Delta r = \frac{m}{A} \quad (2.2)$$

The uncertainty in each parameter was calculated using the standard deviation (equation A.2) of the four measurements per unit, and the total uncertainty was calculated using the approximation of uncorrelated variables used in equation A.13. The conversion from mg per  $\text{cm}^2$  to nuclei per  $\text{cm}^2$  was done numerically, by multiplying the mass density with Avogadro's number  $N_A$  and dividing by the mol-mass of the target atoms.

After the characterization, each foil was mounted on a plastic frame and attached with capton tape along the edges (from previous experiments, capton tape have shown to be a large **proton?** degrader, so it was important that the tape was not in the beamline **cite article? but which?**). The target frames can be seen in figure 2.3.

### 2.2.2 Irradiation of target stack

The irradiation included tuning of the beam and one hour of radiation over the target stack. Whenever the beam was turned on, the beam tube had to be pumped down to a vacuum, to not attenuate the beam.

---

<sup>3</sup>(Syed M. Qaim. Nuclear data for production and medical application of radionuclides: Present status and future needs. Nuclear Medicine and Biology, 44:31–49, jan 2017.)

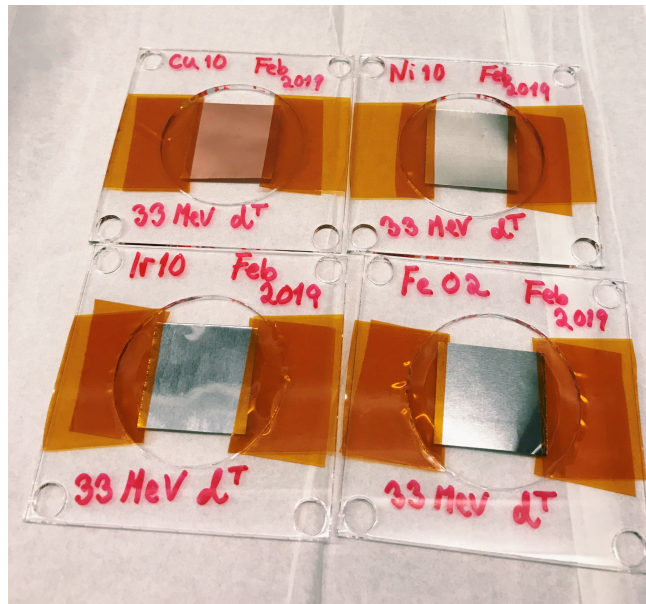


Figure 2.3: The figure shows the four different targets mounted on plastic frames with capton tape attached along the edges of the foils.

### Tuning the beam

The cyclotron was tuned for a 33 MeV deuteron beam, and needed to have the correct beam spot. First, the beam spot was visualized using a ca. 2.5 cm thick borosilicate glass, painted with a mixture of phosphor powder and vacuum grease (so that the paint does not evaporate as the tube was pumped down to vacuum). When ionizing radiation strikes the phosphor, the phosphor is excited and emits light in the de-excitation, called phosphorescence. The glass is placed on the end of the beam tube. With a camera placed in cave 0, from the control room, the beam could be steered to be centered and ca. 1 cm in diameter. Secondly, visualization of the beam throughout the beam stack was important to see that the beam did not diverge converge/diverge or move in the wrong direction over the target stack. Gafchromic films which change color if struck by ionizing radiation was placed in the front and the back of the target holder. The films were exposed for a brief second, and the blue spot was evaluated. This was done until the beam gave good results both in the front and in the back of the stack.

The beam efficiency transmission was calculated by measuring the current at the Faraday cup right after the cyclotron vault (BS-02) and right before cave 0 (FC-01). BS-02 was measured to be 420 nA and FC-01 was measured to be 285 nA. This gave beam efficiency of transmission

$$\frac{FC - 01}{BS - 02} = 67\%$$

### Irradiation of the target stack

The targetstack was irradiated for exactly an hour, and the current was read of the beam integrator evenly, to assure that the it increased constantly. The beamcurrent from the beam integrator read 128.5 nA. Right after end of beam, the targets were sealed in plastic bags to avoid contamination. The foils were counted at the seven different detectors for the following 4 weeks after end of beam, first short counts to get as many observations as possible of the short-lived activities and longer and longer counts as the times since end of beam passes, so that the counting statistics for the longer lived activites are good.

Table 2.1: Characterization of each foil, along with calculated mass density. Each length is measured in mm, and mass in grams.

Foil	Length1 (mm)	Length2 (mm)	Thickness (mm)	Mass (g)	Mass density (mg/cm <sup>2</sup> )
SS1	...				
Ni01	25.228	25.293	0.0285	0.1453	22.772 ± 0.138
Ir01	24.943	24.968	0.0295	0.3436	55.174 ± 0.053
Cu01	25.553	24.883	0.0341	0.1420	22.338 ± 0.048
Fe01	24.400	26.068	0.0278	0.1274	20.030 ± 0.110
Ni02	25.288	25.428	0.0295	0.1487	23.118 ± 0.096
Ir02	24.923	25.005	0.0278	0.3465	55.601 ± 0.238
Cu02	25.443	25.550	0.0348	0.1451	22.325 ± 0.028
Fe02	25.525	23.800	0.0274	0.1216	20.017 ± 0.034
Ni03	25.295	25.210	0.0270	0.1425	22.338 ± 0.066
Ir03	24.885	24.983	0.0243	0.3459	55.643 ± 0.121
Cu03	25.560	25.508	0.0343	0.1455	22.313 ± 0.043
Fe03	26.113	25.235	0.0310	0.1315	19.948 ± 0.114
Ni04	25.303	24.888	0.0273	0.1304	20.704 ± 0.068
Ir04	24.960	24.833	0.0261	0.3471	56.000 ± 0.109
Cu04	25.153	25.603	0.0333	0.1435	22.284 ± 0.027
Ni05	25.325	25.495	0.0263	0.1406	21.768 ± 0.045
Ir05	24.948	24.958	0.0256	0.3435	55.161 ± 0.081
Cu05	25.213	25.573	0.0334	0.1447	22.443 ± 0.028
Ni06	25.530	25.195	0.0285	0.1471	22.861 ± 0.123
Ir06	24.760	24.960	0.0240	0.3444	55.731 ± 0.088
Cu06	25.343	25.513	0.0340	0.1448	22.396 ± 0.012
Ni07	25.338	25.278	0.0268	0.1479	23.092 ± 0.078
Ir07	24.955	25.008	0.0278	0.3538	56.685 ± 0.085
Cu07	25.625	25.248	0.0326	0.1444	22.320 ± 0.014
Ni08	25.205	24.950	0.0256	0.1409	22.409 ± 0.124
Ir08	24.723	24.985	0.0281	0.3585	58.030 ± 0.130
Cu08	25.370	24.885	0.0333	0.1414	22.401 ± 0.033
Ni09	25.220	25.378	0.0257	0.1392	21.741 ± 0.073
Ir09	24.670	24.993	0.0273	0.3494	56.669 ± 0.043
Cu09	25.390	26.455	0.0331	0.1506	22.425 ± 0.041
Ni10	25.285	24.405	0.0271	0.1425	23.093 ± 0.024
Ir10	24.973	24.980	0.0270	0.3435	55.065 ± 0.055
Cu10	25.470	25.338	0.0355	0.1440	22.314 ± 0.047
SS2	...				
P-degrader	...				
Ni neutron monitor	...				

### Intensity profile of the beam

After irradiation, gafchromic film was attached to the activated stainless steel in the front and the back of the stack, to obtain an intensity profile of the beam. The radius of the activity from stainless on gafchromic film is used in the imaging process program Image-J, which can be seen on figure 2.5. The gafchromic films were scanned, and the intensity data (**x and y arrays**) were obtained by inverting the scanned image, and drawing a line segment along the beam spot that automatically created an position dependent intensity array. The intensity profile can be fitted to a Gaussian, which is shown examplewise in figure 2.6, which is the horizontal beam profile in the front and the back of the stack. By measuring the full width half maximum (FWHM) of the beam profile, we were able to build confidence in the size of the beam spot, which was ca. 1 cm in diameter. In the assumption that the beam was underfilled, it was important to build confidence in that we are calculating correctly. The FWHM over SS1 was 1.2017 cm horizontally ( $\sigma^2 = 0.2604 \text{ cm}^2$ ) and 1.1420 cm vertically ( $\sigma^2 = 0.2352 \text{ cm}^2$ ). The FWHM over SS2 was 0.6706 cm horizontally ( $\sigma^2 = 0.0811 \text{ cm}^2$ ) and 0.5783 cm vertically ( $\sigma^2 = 0.0603 \text{ cm}^2$ ).



(a) The target stack in target holder      (b) Target holder placed in the end of beam tube

Figure 2.4: Figure shows the target stack and how it was placed in the beam tube.

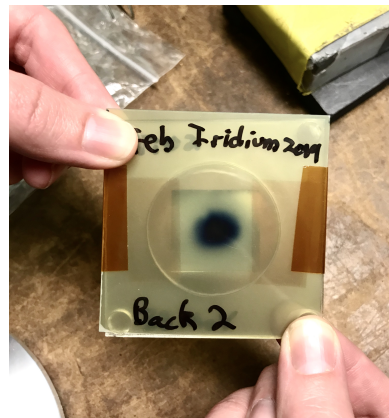
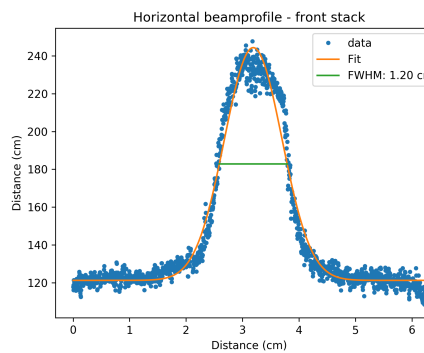


Figure 2.5: The gafchromic film on the activated SS2 foil.

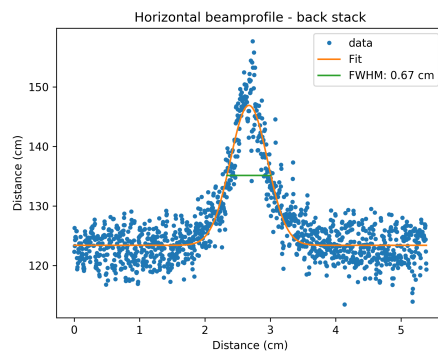
Normally the beam broadens throughout the stack due to scattering. As we can see, this is not the case, since the beam is stopped in the target stack, and therefore we do not know how much the beam truly scatters. This gives a higher uncertainty. The stainless steel (which consists of ..) has fast decay time. However since it emits beta-particles, the radius will slightly increase, and the true beam spot is slightly smaller. Thus the estimated FWHM values for SS1 seem to be within the criterion for underfilled targets.

### 2.2.3 Counting on high purity detectors

Seven different detectors were used, six IDM Ortec detectors (detectors 1-6) with detector diameter 85 mm, detector length 30 mm and hole depth 15 mm, and one Germanium detector (detector 7) with detector diameter 64.9 mm, detector length 57.8 mm and hole depth 48.6 mm [from detector diagrams](#). Besides, IDM detectors are placed in cave 4c (see figure 2.1), which have previously been used as radiation chamber. Thus, background radiation is present. For detector 7, there is lead shielding around the detector. Spectra taken on the Germanium detector is preferred. In order to visualize the



(a) Horizontal intensity profile of SS1



(b) Horizontal intensity profile at SS2

Figure 2.6: Figure shows the intensity profile of the deuteron beam in the front and in the back of the stack horizontally.



Figure 2.7: The calibration point sources that were used in the efficiency calibration of the detector.

Table 2.2: The calibration point sources along with gamma lines used in the calibration of the detectors. \* indicates that the value has been averaged over two peaks with similar energy, less than 1 keV. For the intensity its just added together.

$^{137}Cs$		$^{133}Ba$		$^{152}Eu$	
$E_\gamma$	$I_\gamma$	$E_\gamma$	$I_\gamma$	$E_\gamma$	$I_\gamma$
32.005*	5.63*	53.1622	2.14	121.7817	28.53
36.3405*	1.02*	80.9979	32.9	244.6979	7.55
661.657	85.10	160.6120	0.638	295.9387	0.440
		223.2368	0.453	344.2785	26.5
		276.3989	7.16	367.7891	0.859
		302.8508	18.34	411.1165	2.237
		356.0129	62.05	244.4853*	3.125*
		383.8485	8.94	503.467	0.1524
				586.2648	0.455
				678.623	0.473
				688.670	0.856
				719.353*	0.345*
				778.9045	12.93
				810.451	0.317
				867.380	4.23
				963.712*	14.65*
				1112.076	13.67
				1212.948	1.415
				1299.142	1.633
				1408.013	20.87

signal from the detector, Maestro (Multichannel Analyzer Emulation Software<sup>4</sup>) was used.

The foils were counted for ca. four weeks following end of beam, with short counts in the beginning to have good statistical data for the short-lived activities, and longer and longer counts as the shorter and medium-lived activities decayed out, to have good statistics (enough counts).

---

<sup>4</sup><https://www.ortec-online.com/products/application-software/maestro-mca>

# Chapter 3

# Analysis

The value that is provided as cross section is a flux-averaged cross section, which means that the cross section is dependent on the flux-weighted average beam energy. An accurate measure of the cross section as a function of deuteron energy was possible, as the thin foils provides smaller average beam energy intervals, and it makes it possible to have more measurements if thick foils are replaced with several thinner (one single foil represents a single measurement). Thin foils also produce minimal amounts of radioactivity, thus the deadtime of the detector and the dose to humans is low. For charged particles, the stopping power is inversely proportional to their energy<sup>1</sup>, and therefore the energy degradation in thicker foils will be large. For thin targets, we can however assume that the stopping power  $dE/dx \simeq 0$ , and the cross section can be replaced with a differential (normalized) cross section

$$\sigma(E) = \frac{\int \sigma(E) \frac{d\phi}{dE} dE}{\int \frac{d\phi}{dE} dE} \quad (3.1)$$

The energy-limits in the integral can be minimized and the error in the energy for charged particles will be small.

## 3.1 Gamma-ray spectroscopy

The spectra were analyzed in FitzPeakz<sup>2</sup>. The mathematic algorithm in which FitzPeakz is based upon is SAMPO80<sup>3</sup>. The peaks are assumed Gaussian with an exponential tail on both sides of the peak. The exponential tail and Gaussian function are joined so function and first derivative are continuous. The algorithm searches for peaks by using the smooth second difference (derivative?) Particularly good for detecting small peaks on a high or low background. The peak areas are calculated by fitting the precalibrated modified Gaussian to the data with a weighted least squares formula using a parabolic background. Fitting intervals are determined automatically by the program. Peaks separated by less than 4 times the average fwhm are fitted together.

For each spectra, a report file containing peak energy, centre channel, full width half maximum, significance, goodness of fit, peak area, uncertainty in peak area, gammas per second, uncertainty in gammas per second and a background estimation for each peak was provided. The most important parameters were the energy, the peak area  $N_C$  and uncertainty in peak area. Peak area was needed for the activity calculation in equation 1.30 which is an important parameter in the calculation of the cross section (equation ??), and in the calculation of the efficiency for the calibration sources (equation 3.2). Gammas per second (also called countrate) was used to get an indication if the rate

<sup>1</sup>Andrew S. Voyles, Lee A. Bernstein, Eva R. Birnbaum, Jonathan W. Engle, Stephen A. Graves, Toshihiko Kawano, Amanda M. Lewis, and Francois M. Nortier. Excitation functions for (p,x) reactions of niobium in the energy range of  $E_p = 40\text{--}90$  MeV. Nuclear Instruments and Methods in Physics Research Section B: Beam Interactions with Materials and Atoms, 429:53–74, aug 2018.

<sup>2</sup><https://www.jimfitz.co.uk/fitzpeak.htm>

<sup>3</sup>[https://sci-hub.tw/https://doi.org/10.1016/0029-554X\(81\)90209-3](https://sci-hub.tw/https://doi.org/10.1016/0029-554X(81)90209-3)

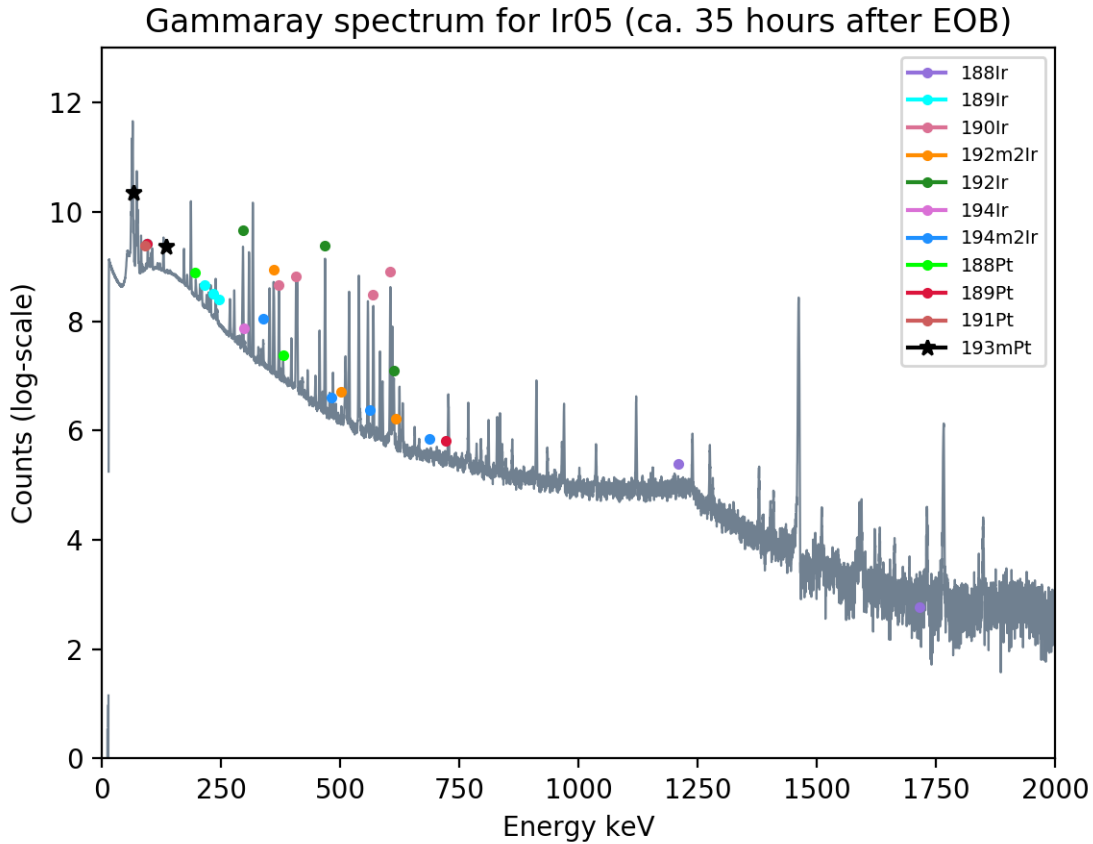


Figure 3.1: Gammaray spectrum for Ir05 taken approximately 35 hours after end of beam. Nuclei does not necessarily represent what is in the peak, but where the peak would have been. Hard to include all since there are different decay times.

of gammas, which were used as a critical tool to evaluate for instance background peaks, or if the activity was too high in comparison to other spectra measured at other detectors.

Figure 3.1 shows an example of a gamma ray spectrum for one of the iridium spectra (Ir05) approximately 35 hours after end of beam. Figure 3.2 shows the X-ray region and gamma region of  $^{193m}\text{Pt}$ .

### Energy and peak-shape calibration

Don't remember exactly how we did this... Used the calibration sources, but did we do an efficiency calibration here? Used calibration sources  $^{137}\text{Cs}$  ( $t_{1/2} = 30.08$  years[?]),  $^{133}\text{Ba}$  ( $t_{1/2} = 10.551$  years[?]) and  $^{152}\text{Eu}$  ( $t_{1/2} = 13.517$  years[?]), which can be seen on figure 2.7.

The calculated peak locations and areas are finally corrected with energy and efficiency calibration data to yield peak energies and intensities. For the energy calibration, linear interpolation on a linear scale and for the efficiency calibration linear interpolation on a log-log scale are used in this code. Calibration errors are added to the peak location and intensity errors to give the final result (p.94). The peak shape calibration uses 7 parameters; two background peaks, peak height and location, peak width, distance from peak centroid to the starting point of exponential on either side. The minimization of the least-squares expression to solve for the peak parameters is done by a subroutine package with an iterative gradient algorithm utilizing the variable metric method. Minimization is terminated when all components in the next step change by less than  $10^{-8}$ , if four succeeding values of  $\chi^2$  are the same or if 100 iterations have been completed. The performed shape calibration can be checked with a few parameters, goodness of fit,  $\chi^2$  per degree of freedom, sigma and error correlation. Sigma below 5 and error correlation between -1 and 1 are acceptable values. (p.90)

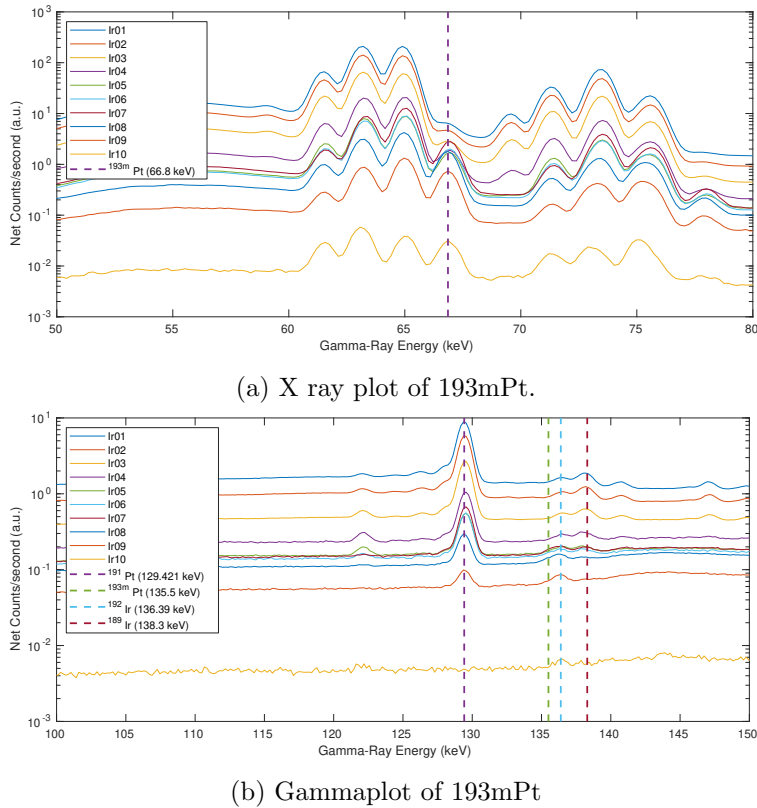


Figure 3.2: Which spectra are these??

From the webpage [jim-fitz.com/calib.html](http://www.jim-fitz.com/calib.html): Each detector was calibrated with peak shape and energy for the calibration sources. Fitzpeakz takes in energy (.enc) and peak shape (.shp) calibration source files, containing the energies listed in table 2.2. For the peak shape, the program determines the parameters of width and the amount of low energy tailing. The energy calibration and peak shape calibration was estimated to a 1st order function.

## 3.2 Efficiency calibration

The efficiency calibration is an important factor in the calculation of the cross section in equation ???. The detector efficiency is the number of events registered divided by the events emitted by the source. The absolute efficiency can be divided into intrinsic and geometrical efficiency, where the intrinsic efficiency is the number of events registered divided by the number of events hitting the detector. The intrinsic efficiency thus depends on the interaction cross section between incident particle and detector material. For neutral particles, the size of the detector affects the intrinsic efficiency, the larger crystal the larger the probability of interaction is. The geometrical efficiency is the radiation emitted by the source which hits the detector. (Techniques for Nuclear and Particle Physics Experiments. William R. Leo. Second Revised Edition. Springer Verlag Berlin Heidelberg GmbH, New York (1994). p. 121-122 )

The efficiency was measured using calibration point sources  $^{137}\text{Cs}$  ( $t_{1/2} = 30.08$  years[?]),  $^{133}\text{Ba}$  ( $t_{1/2} = 10.551$  years[?]) and  $^{152}\text{Eu}$  ( $t_{1/2} = 13.517$  years[?]). Figure 2.7 shows the calibration points sources ( $^{22}\text{Na}$  was excluded during the data-analysis since it only contains a single gamma-line and gave poorer results). On each calibration source, a reference date is given with an activity, which here is referenced to as  $A_0$  of the calibration sources.

Solving Equation 1.30 for efficiency,  $\epsilon$ , the analytical efficiency as a function of gamma-ray energy and

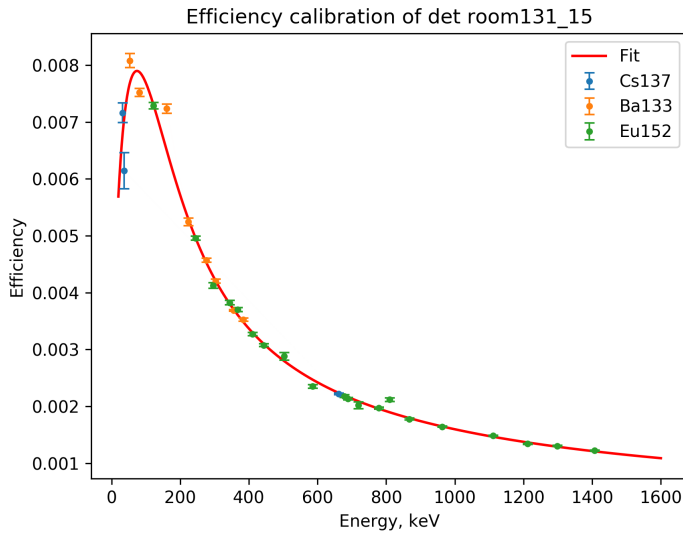


Figure 3.3: An example of an efficiency curve with exact points calculated from equation 3.2 and a curve fit from equation 3.3.

intensity is

$$\epsilon(E_\gamma) = \frac{N_C \lambda}{A_0 I_\gamma (1 - e^{-\lambda \Delta t_c}) e^{-\lambda \Delta t_d}} \quad (3.2)$$

where  $\lambda$  is the decay constant and  $N_C$  is the number of counts in the measured spectra, and  $\Delta t_d$  is the delay time since the reference date. The analytical efficiency gives one single value for the efficiency at energy  $E_\gamma$ , but we want a continuous function which gives the efficiency at any gamma-energy. A model based upon Gallagher, W. J., Cipolla, S.J. (1974) was applied which takes the probability of penetration through the deadlayer of the detector and the probability of interaction in the detector volume into account

$$\epsilon(E_\gamma) = B_0 + \underbrace{(e^{-B_1 E_\gamma^{B_2}})}_{\text{dead layer}} \underbrace{(1 - e^{-B_3 E_\gamma^{B_4}})}_{\text{interacting with volume}} \quad (3.3)$$

where  $B_i$  is optimum parameters minimizing the  $\chi^2$  in the scipy optimizing curve fit function<sup>4</sup>). Figure 3.3 shows an example of an efficiency curve for a detector at a specific distance from the detector. The uncertainty of the efficiency was estimated using equation A.6 numerically. For each source, the gamma-lines with the intensities which were used to calculate the efficiency points for each source is listed in table 2.2.

### 3.3 End of beam activities

The end of beam activities were estimated by extrapolating backwards in time, with the measured activities at various timepoints after the end of beam. The activities as a function of time sine EOB was calculated using equation 1.29, along with a self-attenuation correction:

$$A(\Delta t_d) = \frac{N_C \lambda}{\epsilon_\gamma (1 - e^{-\lambda \Delta t_d}) e^{-\mu \rho \Delta r / 2}} \quad (3.4)$$

where  $\mu$  is the attenuation coefficient<sup>5</sup>, and  $\rho \Delta r$  is the mass density of the foil. The gammas which were used are listed in tables A.2, A.1, A.4 and A.3 for iron, nickel, copper and iridium respectively. The self-attenuation correction is based on the assumption that all activity that is made is located

<sup>4</sup>[https://docs.scipy.org/doc/scipy/reference/generated/scipy.optimize.curve\\_fit.html](https://docs.scipy.org/doc/scipy/reference/generated/scipy.optimize.curve_fit.html)

<sup>5</sup><https://www.nist.gov/pml/xcom-photon-cross-sections-database>

midway in the foil thicknesses. In reality however, the activity profile will follow the same shape as the excitation function over the energy range that expands over the foil (since activity and cross section are proportional). We do not know the excitation function ahead of time, and the excitation function does not change much either, since the foil thicknesses are so thin. So instead, this simplification is done, assuming that the average attenuation is through half of the foil thickness.

The equation describing the shape of the decay curve is given in equation 1.18 for single decay or 1.19 for multiple decay. Decay chains of single and two-step decay ( $n=1,2$ ) was sufficient in this analysis;

$$A = A_0 e^{-\lambda \Delta t_d}, \quad \text{single step decay} \quad (3.5)$$

and

$$A_2(t) = \lambda_n \left[ A_{1,0} \lambda_1 \frac{(e^{-\lambda_1} + e^{-\lambda_2})}{\lambda_1 - \lambda_2} + A_{2,0} e^{-\lambda_2 t} \right], \quad \text{two step decay} \quad (3.6)$$

where subnumber 1 is the parent nucleus, and subnumber 2 is the daughter nucleus. Parent activity is calculated from single step decay. The uncertainty was treated as **covarianced variables?**

The way in which the extrapolation was done was the `scipy optimize curve fit` function, where the  $A_0$  of the daughter was the optimizing parameter. Since there is only one optimized parameter, there was no covariance and the uncertainty was calculated using equation A.13. In the cases where neither parent or daughter activity were known, which were the case for the monitor reaction  $^{58}Co$  with  $^{58m}Co$  decaying into the ground state by internal conversion, both parent and daughter activity were optimizing parameters which are very correlated and thus the uncertainty in end of beam activity was calculated A.6. Figure 3.4 shows two examples of the two different activity curves; one step decay for  $^{193m}Pt$  ( $t_{1/2}=4.33$  days) and two step decay for the monitor product  $^{58}Co$  ( $t_{1/2}=70.86$  days) with feeding from the isomer  $^{58m}Co$  ( $t_{1/2}=9.10$  hours).

### 3.4 Energy and Beam current

For the equation for cross section (equation 1.45), the beam current  $\Phi(E)$  must be known. The beam integrator measured 128.5 nA, which is the current entering the stack. However, due to large energy degradation in the energy stack, there will be a certain spread of the beam, following scattering. In addition, there have not been an experiment with deuterium on a target stack before, so we also needed to see how much deuteron break up affected the current throughout the stack. Monitor reactions are reactions with well-known cross sections<sup>6</sup>. The IAEA recommended cross sections for  $^{nat}Fe(d,x)^{56}Co$ ,  $^{nat}Ni(d,x)^{61}Cu$ ,  $^{nat}Ni(d,x)^{56,58}Co$  and  $^{nat}Cu(d,x)^{62,63,65}Zn$  (**write about Q value, half life**) were used to estimate a more sensitive deuteron beam current throughout the stack. By solving 1.45 for beam current, the beamcurrent throughout the stack can be estimated

$$\Phi(E) = \frac{A_0}{N_T(1 - e^{-\lambda \Delta t_{irr}})\sigma(E)_{mon}} \quad (3.7)$$

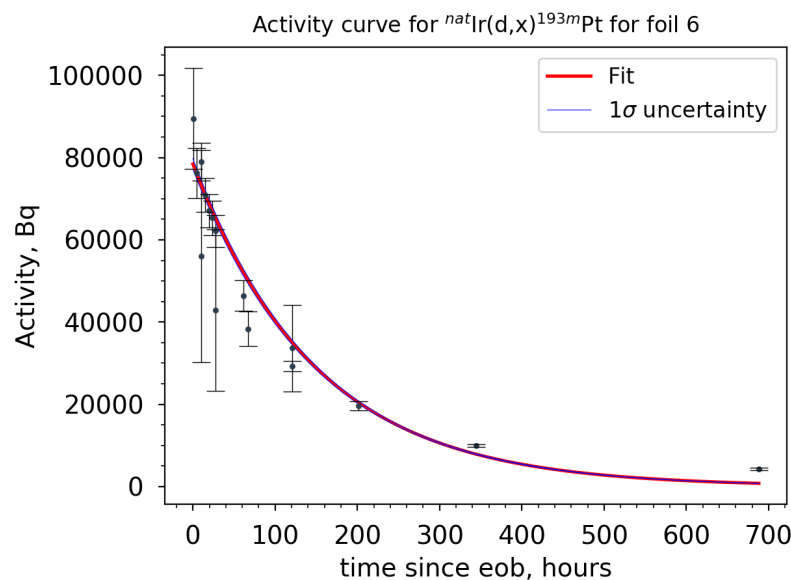
In cross section experiments using thin targets<sup>7</sup>, the suggested value is a flux average cross section, which implies that the cross section is dependent on the flux-weighted average beam energy. One single foil thus provides one cross section measurement, with the uncertainty in energy only being dependent on the energy distribution in each foil. For thin targets, a stopping power  $dE/dx = 0$  is assumed which is a very good approximation for targets which are less than 50 mg/cm<sup>2</sup> **cite?**

Normalized differential beam current (**need some help understanding this in detail**)

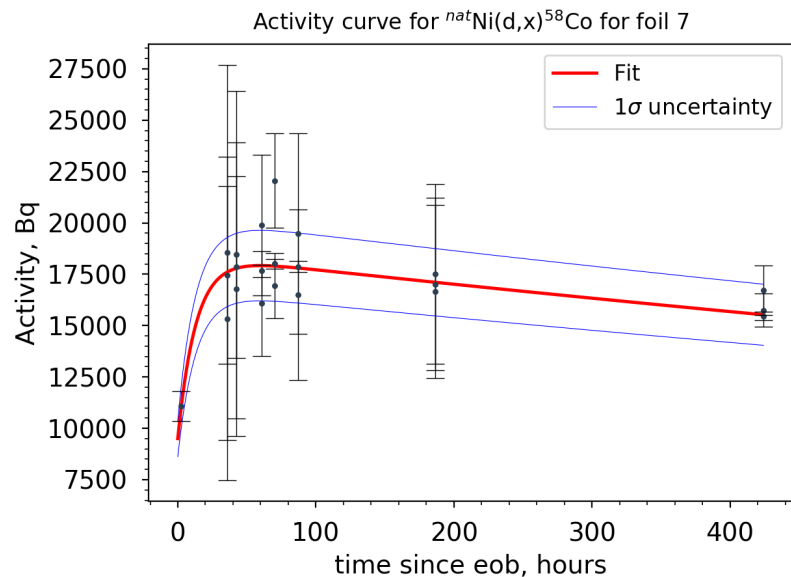
$$\sigma(E)_{mon} = \frac{\int \sigma(E) \frac{d\phi}{dE} dE}{\int \frac{d\phi}{dE} dE} \quad (3.8)$$

<sup>6</sup>[https://www-nds.iaea.org/medical/monitor\\_reaction\\_article.pdf](https://www-nds.iaea.org/medical/monitor_reaction_article.pdf)

<sup>7</sup>Special curriculum p. 14



(a) Activity of  $^{193m}\text{Pt}$  ( $t_{1/2}=4.33$  d) produced from iridium. The end of beam activity was estimated using a one step decay (equation 3.5)



(b) Activity of  $^{58}\text{Co}$  ( $t_{1/2}=70.86$  d) produced from nickel. The end of beam activity is estimated using a two step decay (equation 3.6. The feeding is from  $^{58m}\text{Co}$  ( $t_{1/2}=9.10$  h.)

Figure 3.4: Two examples of activity curves.

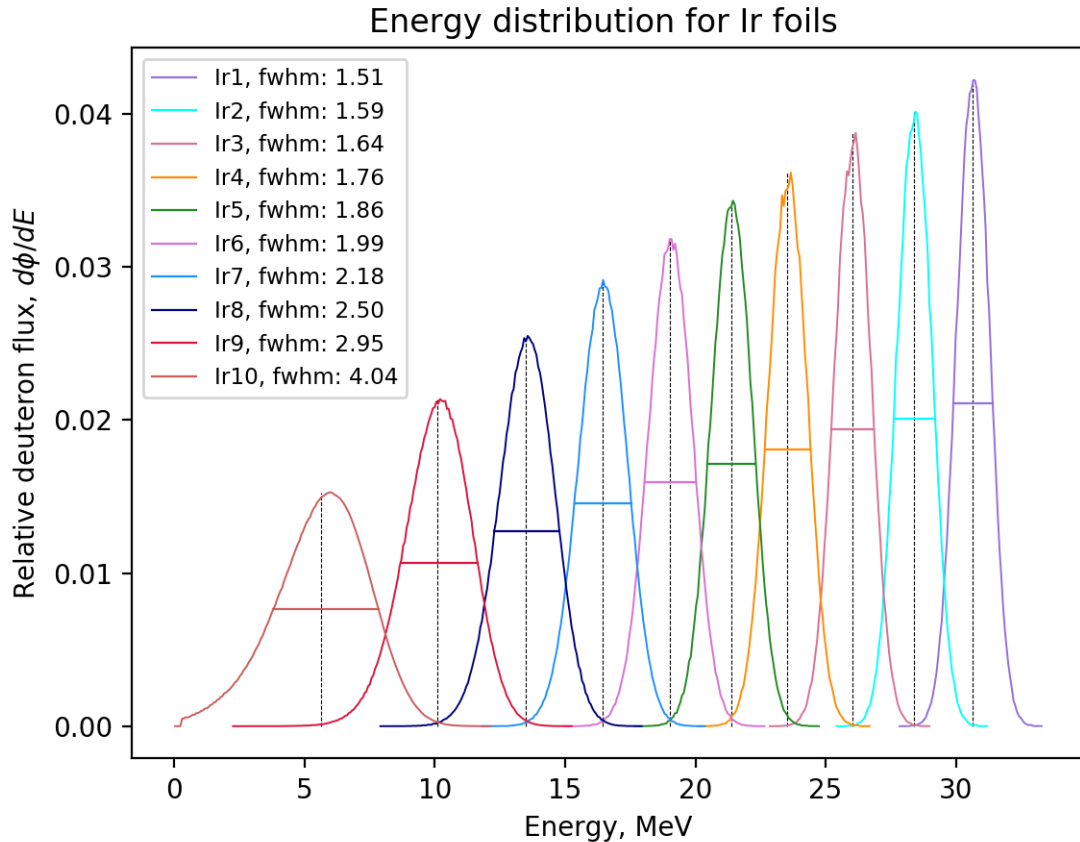


Figure 3.5: Iridium energy flux distribution over the 10 foils. As the energy degrades, skewed and larger full width half max. The vertical line in each peak is the mean value. This indicates that at lower energies, the right uncertainty is greater than the left uncertainty in the peak. **Why does peak have low energy tail?**

where  $\sigma(E)$  is the IAEA recommended cross section,  $\frac{d\phi}{dE}$  is the energy dependent deuteron flux through each foil. The deuteron flux (or energy degradation) was estimated using a code called NPAT's (nuclear physics analysis tool) Ziegler simulation<sup>8</sup>. NPAT uses the Anderson & Ziegler formalism for calculating charged-particle stopping powers in matter in a stack with targets. **write a few sentences about this in the theory!**. The code thus simulates the deuteron flux as a function of energy in the beam stack (assigned to a foil).

Figure 3.5 shows an overview of the flux-energy distribution in each foil for Iridium. The other monitor foils have the same functions. **Write about recommended data, the spline function etc etc.. need some info from andrew here**

### 3.4.1 Variance minimization

From Niobium paper p. 57: In theory, the beam current should be more or less constant through the stack, even though the deuterons lose energy. Variance minimization is a technique to reduce the uncertainty in the deuteron beam energies. Non-consistent values for the beam current further back in the stack can be wrong energy bin assignments in the modeled energy distribution (ziegler), or a systematic error in the areal density, which gets progressively worse further back in the stack, "due to the compound effect of systematic uncertainties in stack areal densities". The areal density and the beam energy was varied with 20% increase and decrease, and the reduced  $\chi^2$  (equation A.4) was estimated over compartment 3, 6 and 9. For compartment 3 ( $E_d \simeq 25$  MeV) all seven monitor reactions were above threshold, thus 6 degrees of freedom. However, early in the target stack, the

<sup>8</sup><https://pypi.org/project/npat/>

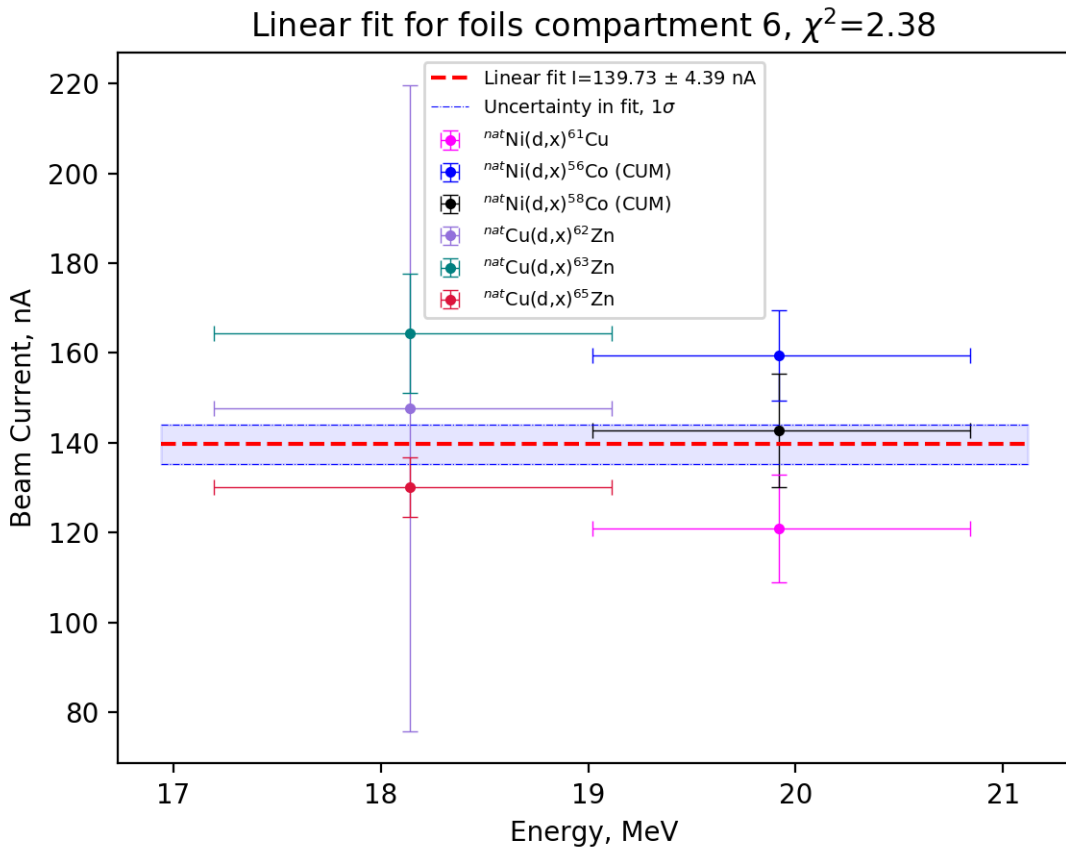
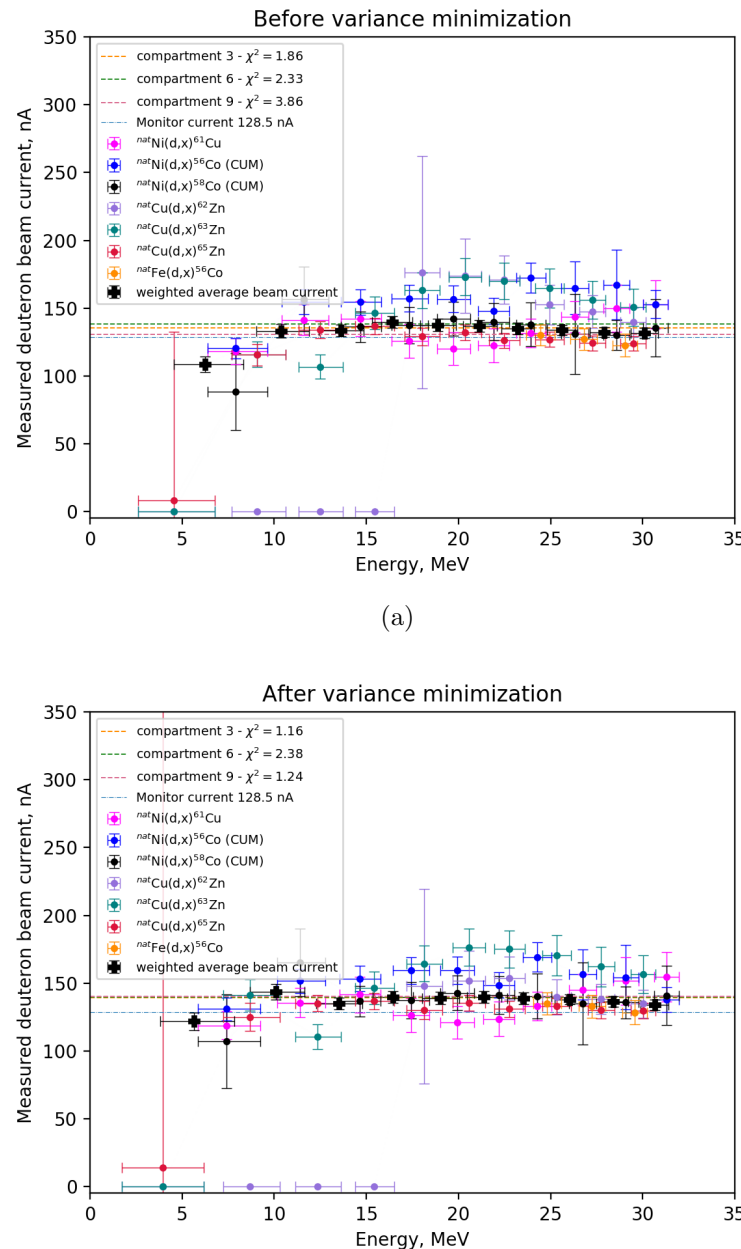


Figure 3.6: The estimated (uncertainty weighted) beamcurrent over compartment 6.

scattering was low, and the  $\chi^2$  does not tell how well the energy bin assignment work further back in the stack. For compartment 6 ( $E_d \simeq 18$  MeV), all the six possible monitor reactions (from nickel and copper) were above threshold, and it gave a good estimate of how the beam current was developing throughout the stack. In compartment 9 ( $E_d \simeq 10$  MeV), five monitor reactions are above threshold (except for  $^{62}\text{Zn}$ ). At the very end it is possible to see the full effect of the scattering.

The beamcurrent loss is assumed zero in one compartment, so a linear beam current fit would have a slope equal to zero. The estimated beam current in each compartment was estimated using the scipy curve fit function, with a straight line as model. Figure 3.6 shows the uncertainty weighted linear fit over compartment 6.

Figure 3.7 shows the beam current before and after variance minimization. After variance minimization, the beam current estimated in each compartment (stabled lines) were similar, and meanwhile the weighted  $\chi^2$  was about the same in compartment 6, it has improved in compartment 3 and very visible in compartment 9. In general the points are also more aligned.



(b) A 2% increase in beam current and a 4.25% increase in areal density gave the overall most consistant beam current, with reasonable values for the weighted .

Figure 3.7: Beam current before and after variance minimization.

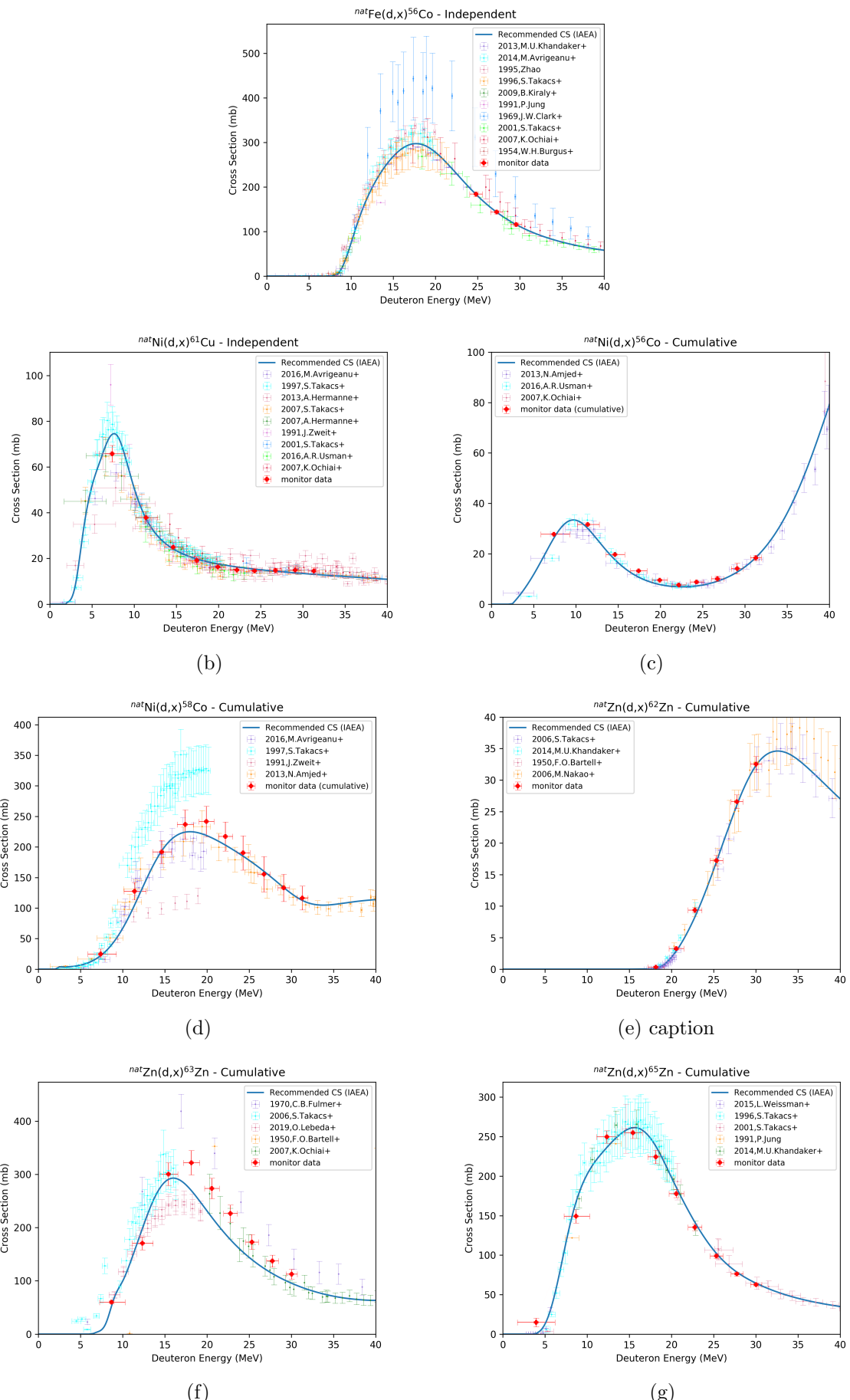


Figure 3.8: Figure shows the estimation of monitor cross section using the calculated beam current. It is compared along with the monitor data.

# Appendix A

## Statistics

Uncertainty in statistics refers to the standard deviation of the data, which gives a number of the spreading of the data from the mean value of the data citation. The variance is the standard deviation squared, which weights the variables to a higher degree.

$$std = \sqrt{\sigma^2} \quad (\text{A.1})$$

$$\sigma = \sqrt{\frac{1}{N} \sum_{i=1}^N (x_i - \bar{x})^2} \quad (\text{A.2})$$

where N is the number of measurements,  $x_i$  is a measurement and  $\bar{x}$  is the average over all measurements.

$\chi^2$  is an estimation of the goodness of the fit, which includes the weight of the error

$$\chi^2 = \sum_i^n \left( \frac{y_i - \bar{y}}{\sigma_i} \right)^2 \quad (\text{A.3})$$

where  $\bar{y}$  is the mean value of y and  $\sigma_i$  is the error in  $y_i$ . The reduced  $\chi^2$  is defined as the  $\chi^2$  per degree of freedom

$$\chi_\nu^2 = \frac{\chi^2}{\nu} \quad (\text{A.4})$$

where  $\nu$  is the degrees of freedom equal to the number of observations minus the number of fitted parameters. A value close to  $\chi_\nu^2 = 1$  indicates that the observations and fit is in well accordance to the error, while  $\chi_\nu^2 > 1$  indicates an underfitting and a  $\chi_\nu^2 < 1$  indicates an overfitting<sup>1</sup>.

A function  $f$  with input  $x$  and a set of variables  $\vec{\beta} = \beta_1, \beta_2, \dots, \beta_n$  and output y can be written on the following form

$$y = f(x, \vec{\beta}) \quad (\text{A.5})$$

The uncertainty in y is dependent on the uncertainty in the different input variables  $\vec{\beta}$ . The matrix expression for error propagation is (Tellinghuisen, Joel, Statistical error propagation)<sup>2</sup>

$$\sigma_y^2 = \mathbf{J} \cdot \mathbf{V} \cdot \mathbf{J}^T \quad (\text{A.6})$$

where  $\sigma_y^2$  is the variance in y, J is the Jacobian matrix

$$\mathbf{J} = \begin{bmatrix} \frac{\partial f}{\partial \beta_1} & \frac{\partial f}{\partial \beta_2} & \dots & \frac{\partial f}{\partial \beta_n} \end{bmatrix} \quad (\text{A.7})$$

and V is the variance-covariance matrix

---

<sup>1</sup>[https://en.wikipedia.org/wiki/Reduced\\_chi-squared\\_statistic](https://en.wikipedia.org/wiki/Reduced_chi-squared_statistic)

<sup>2</sup>A full derivation of the expression can be found in Uncertainty Propagation for Measurements with multiple output quantities, Dobbert, Schrijver

$$\mathbf{V} = \begin{bmatrix} \sigma_0^2 & \sigma_{0,1} & \cdots & \sigma_{0,n} \\ \sigma_{1,0} & \sigma_1^2 & \cdots & \sigma_{1,n} \\ \vdots & \vdots & \ddots & \vdots \\ \sigma_{n,0} & \sigma_{n,1} & \cdots & \sigma_n^2 \end{bmatrix} \quad (\text{A.8})$$

In the cases where the input parameters are uncorrelated, all non-diagonal elements in the variance-covariance matrix is equal to zero, and the expression for the variance is simplified to

$$\sigma_y^2 = \sum_{i=1}^n \left( \frac{\partial f}{\partial \beta_i} \right)^2 \sigma_{\beta_i}^2 \quad (\text{A.9})$$

Whenever the input parameters are correlated, which means that  $\sigma_{\beta_i, \beta_j} \neq 0$ , we have to apply equation A.6, otherwise, the simplification in equation A.9 will give wrong error propagation.

To evaluate the partial derivatives of  $f$ , the computational derivation is applicable

$$\frac{\partial f}{\partial \beta_i} \approx \frac{f(x, \beta_i + \frac{\Delta \beta_i}{2}) - f(x, \beta_i - \frac{\Delta \beta_i}{2})}{\Delta \beta_i} \quad (\text{A.10})$$

where  $\Delta \beta_i$  is a small number, like  $10^{-8} \beta_i$ .

For a function  $f = xy$ , the variance can be expressed from equation A.6, where

$$\mathbf{J} = [y \ x]$$

and

$$\mathbf{V} = \begin{bmatrix} \sigma_x^2 & \sigma_{x,y} \\ \sigma_{y,x} & \sigma_y^2 \end{bmatrix}$$

$$\sigma_f^2 = x^2 \sigma_y^2 + y^2 \sigma_x^2 + 2xy \sigma_{x,y} \quad (\text{A.11})$$

If we multiply each term so that we can collect  $f^2$  in the numerator, the variance in  $f$  can be expressed as

$$\sigma_f^2 = f^2 \left( \frac{\sigma_x^2}{x^2} + \frac{\sigma_y^2}{y^2} + \frac{2\sigma_{x,y}}{xy} \right) \quad (\text{A.12})$$

if the variables  $x$  and  $y$  are uncorrelated, the variance is further simplified, and more terms can be included easily. The simplified standard deviation of a function  $f(\bar{\beta}) = \beta_1 \cdot \beta_2 \cdots \beta_n$  with uncorrelated variables is thus

$$\sigma_f = |f| \sqrt{\left( \frac{\sigma_{\beta_1}}{\beta_1} \right)^2 + \left( \frac{\sigma_{\beta_2}}{\beta_2} \right)^2 + \cdots + \left( \frac{\sigma_{\beta_n}}{\beta_n} \right)^2} \quad (\text{A.13})$$

# Appendix A

## Tables

For all tables, the assumption is that the main particle emission is due to alpha, proton or neutron emission. However, triton,  $^3\text{He}$  and deuterons are still fed when above threshold, but from theory, the feeding is low. For triton,  $^3\text{He}$  and deuteron respectively, subtract 8.5, 7.7 or 2.2 respectively from the Q value. Alphaparticles (due to the large binding energy and spin equal to 0) will be more fed. To calculate Q value for alpha emission subtract 28.3 MeV from Q value of 2p2n-reactions. Q values from <sup>1</sup> are used. Q values below 40 MeV are included for comparison to experimental data.

### A.1 Product nuclei

Table A.1: Products observed on Nickel foils. Nickel has five stable isotopes:  $^{58}\text{Ni}$  (68.077%),  $^{60}\text{Ni}$  (26.223 %),  $^{61}\text{Ni}$  (1.1399%),  $^{62}\text{Ni}$  (3.6346%) and  $^{64}\text{Ni}$  (0.9255%). If the nucleus has provided energy level, the nucleus is an isomer, if nothing then ground state. **The table is inspired by Tarkanyi et al 2019 (ir paper)**

Nuclide level (keV)	Half life	Decay mode	Reaction route	Q value (keV)	$E_\gamma$ (keV)	$I_\gamma$ (%)
$^{52}\text{Mn}$ (0.0)	5.591 d 21.1 m	$\epsilon : 100\%$	$^{58}\text{Ni}(\text{d},2\alpha)$	-1235.6	744.233	90.0
			$^{60}\text{Ni}(\text{d},2\text{n}2\alpha)$	-21622.6	935.544	94.5
			$^{61}\text{Ni}(\text{d},3\text{n}2\alpha)$	-29442.7	1246.278	4.21
					1434.092	100.0
$^{54}\text{Mn}$ (0.0)	312.20 d	$\epsilon : 100\%$	$^{58}\text{Ni}(\text{d},2\text{p}\alpha)$	-8538.3	834.848	99.9760
			$^{60}\text{Ni}(\text{d},2\alpha)$	-629.6		
			$^{61}\text{Ni}(\text{d},\text{n}2\alpha)$	-8449.7		
			$^{62}\text{Ni}(\text{d},2\text{n}2\alpha)$	-19045.4		
$^{59}\text{Fe}$ (0.0)	44.490 d	$\beta^- : 100\%$	$^{60}\text{Ni}(\text{d},3\text{p})$	-12539.5	1291.590	43.2
			$^{61}\text{Ni}(\text{d},\text{n}3\text{p})$	-20359.6		
			$^{62}\text{Ni}(\text{d},\text{p}\alpha)$	-2659.7		
			$^{64}\text{Ni}(\text{d},2\text{n}\text{p}\alpha)$	-19154.9		

<sup>1</sup><https://www.nndc.bnl.gov/qcalc/>

## APPENDIX A. TABLES

$^{55}\text{Co}$ (0.0)	17.53 h	$\epsilon : 100\%$	$^{58}\text{Ni}(\text{d},\text{n}\alpha)$ $^{60}\text{Ni}(\text{d},3\text{n}\alpha)$ $^{61}\text{Ni}(\text{d},4\text{n}\alpha)$	-3559.4 -23946.4 -31766.5	91.9 385.4 477.2 520.0 803.7 827.0 931.1 984.6 1212.8 1316.6 1370.0 1408.5 1792.1 2177.6 2872.4	1.16 0.54 20.2 0.83 1.87 0.21 75 0.52 0.26 7.1 2.9 16.9 0.082 0.29 0.118
$^{56}\text{Co}$ (0.0)	77.236 d	$\epsilon : 100\%$	$^{58}\text{Ni}(\text{d},\alpha)$ $^{61}\text{Ni}(\text{d},2\text{n}\alpha)$ $^{61}\text{Ni}(\text{d},3\text{n}\alpha)$ $^{62}\text{Ni}(\text{d},4\text{n}\alpha)$	6522.5 -13864.5 -21684.6 -32280.4	787.743 846.770 977.372 1175.101 1963.741 2015.215 2034.791	0.3111 99.9399 1.421 2.252 0.707 3.016 7.77
$^{58}\text{Co}$ (0.0)	70.86 d	$\epsilon : 100\%$	$^{58}\text{Ni}(\text{d},2\text{n})$ $^{60}\text{Ni}(\text{d},\alpha)$ $^{61}\text{Ni}(\text{d},\text{n}\alpha)$ $^{62}\text{Ni}(\text{d},2\text{n}\alpha)$ $^{64}\text{Ni}(\text{d},4\text{n}\alpha)$	-1823.8 6084.9 -1735.3 -12331.0 -28826.2	810.7593 863.951 1674.725	99.450 0.686 0.517
$^{60}\text{Co}$ (0.0)	1925.28 d	$\beta^- : 100\%$	$^{60}\text{Ni}(\text{d},2\text{p})$ $^{61}\text{Ni}(\text{d},\text{n}2\text{p})$ $^{62}\text{Ni}(\text{d},\alpha)$ $^{64}\text{Ni}(\text{d},2\text{n}\alpha)$	-4265.0 -12085.1 5614.8 -10880.4	1173.228 1332.492	99.85 99.9826
$^{56}\text{Ni}$ (0.0)	6.075 d	$\epsilon : 100\%$	$^{58}\text{Ni}(\text{d},3\text{np})$	-24688.4	158.38 480.44 749.95 811.85 1561.80	98.8 36.5 49.5 86.0 14.0
$^{57}\text{Ni}$ (0.0)	35.60 h	$\beta^+ : 100\%$	$^{58}\text{Ni}(\text{d},2\text{np})$ $^{60}\text{Ni}(\text{d},4\text{np})$	-14440.8 -34827.8	379.94 673.44 906.98 1046.68 1224.00 1377.63 1730.44 1757.55 1897.42 1919.52 2133.04 2804.20	0.0670 0.0491 0.0613 0.134 0.063 81.7 0.052 5.75 0.028 12.3 0.0286 0.098
$^{65}\text{Ni}$ (0.0)	2.51719 h	$\beta^- : 100\%$	$^{64}\text{Ni}(\text{d},\text{p})$	3873.51	366.27 1481.84 1623.42 1724.92	4.81 23.59 0.498 0.399

$^{60}\text{Cu}$ (0.0)	23.7 m	$\epsilon : 100\%$	$^{60}\text{Ni}(\text{d},2\text{n})$ $^{61}\text{Ni}(\text{d},3\text{n})$ $^{62}\text{Ni}(\text{d},4\text{n})$	-9134.9 -16955.0 -27550.7	467.3 497.9 643.2 952.4 1035.2 1110.5 1293.7 1791.6 1861.6 1936.9 2061.0 2158.9 2403.3 2687.9 2746.1	3.52 1.67 0.97 2.73 3.70 1.06 1.85 45.4 4.8 2.20 0.79 3.34 0.77 0.44 1.06
$^{61}\text{Cu}$	3.339 h	$\epsilon : 100\%$	$^{60}\text{Ni}(\text{d},\text{n})$ $^{61}\text{Ni}(\text{d},2\text{n})$ $^{62}\text{Ni}(\text{d},3\text{n})$ $^{64}\text{Ni}(\text{d},5\text{n})$	2575.3 -5244.8 -15840.5 -32335.7	282.956 373.050 529.169 588.605 625.605 656.008 816.692 841.211 902.294 1032.162 1073.465 1132.351 1185.234 1446.492	12.2 2.1 0.38 1.17 0.040 10.8 0.31 0.21 0.083 0.043 0.033 0.090 3.7 0.045
$^{64}\text{Cu}$	12.701 h	$\epsilon : 100\%$ $\beta^- : 38.5\%$	$^{64}\text{Ni}(\text{d},2\text{n})$	-4681.3	1345.77	0.475

## APPENDIX A. TABLES

---

Table A.2: Products observed on Iron foils. Iron has five stable isotopes:  $^{54}\text{Fe}$  (5.845%),  $^{56}\text{Fe}$  (91.754 %),  $^{57}\text{Fe}$  (2.119%) and  $^{58}\text{Fe}$  (0.282%). If the nucleus has provided energy level, the nucleus is an isomer, if nothing then ground state. **The table is inspired by Tarkanyi et al 2019 (ir paper)**

Nuclide level (keV)	Half life	Decay mode	Reaction route	Q value (keV)	$E_\gamma$ (keV)	$I_\gamma$ (%)
$^{48}\text{V}$ (0.0)	15.9735 d	$\epsilon : 100\%$	$^{54}\text{Fe}(\text{d},2\alpha)$	-3490.9	944.130	7.870
			$^{56}\text{Fe}(\text{d},2\text{n}2\alpha)$	-23986.1	983.525	99.98
			$^{57}\text{Fe}(\text{d},3\text{n}2\alpha)$		1312.106	98.2
$^{51}\text{Cr}$ (0.0)	27.704 d	$\epsilon : 100\%$	$^{54}\text{Fe}(\text{d},\text{p}\alpha)$	-1381.3	320.0824	9.910
			$^{56}\text{Fe}(\text{d},2\text{n}\alpha)$	-21876.5		
			$^{57}\text{Fe}(\text{d},3\text{n}\alpha)$	-29522.6		
			$^{58}\text{Fe}(\text{d},4\text{n}\alpha)$	-39567.2		
$^{52}\text{Mn}$ (0.0)	5.591 d d	$\epsilon : 100\%$	$^{54}\text{Fe}(\text{d},\alpha)$	5163.6	346.02	0.980
			$^{56}\text{Fe}(\text{d},2\text{n}\alpha)$	-15331.6	744.233	90.0
			$^{57}\text{Fe}(\text{d},3\text{n}\alpha)$	-22977.7	848.18	3.32
					935.544	94.5
					1246.278	4.21
					1333.649	5.07
					1434.092	100.0
$^{54}\text{Mn}$ (0.0)	312.20 d	$\epsilon : 100\%$	$^{54}\text{Fe}(\text{d},2\text{p})$	-2139.1	834.8480	99.9760
			$^{56}\text{Fe}(\text{d},\alpha)$	5661.4		
			$^{57}\text{Fe}(\text{d},\text{n}\alpha)$	-1984.7		
			$^{58}\text{Fe}(\text{d},2\text{n}\alpha)$	-12029.3		
$^{53}\text{Fe}$ (0.0)	8.51 m ????	$\epsilon : 100\%$	$^{54}\text{Fe}(\text{d},2\text{np})$	-15602.9	377.9	42%
			$^{56}\text{Fe}(\text{d},4\text{np})$	-36098.1		
$^{59}\text{Fe}$ (0.0)	44.490 d	$\beta^- : 100\%$	$^{58}\text{Fe}(\text{d},\text{p})$	4356.44	1099.245	56.5
					1291.590	43.2
$^{55}\text{Co}$ (0.0)	17.53 h	$\epsilon : 100\%$	$^{54}\text{Fe}(\text{d},\text{n})$	2839.8	91.9	1.16
			$^{56}\text{Fe}(\text{d},3\text{n})$	-17655.4	477.2	20.2
			$^{57}\text{Fe}(\text{d},4\text{n})$	-25301.5	803.7	1.87
					827.0	0.21
					931.1	75
					1316.6	7.1
					1370.0	2.9
					1408.5	16.9
					2177.6	0.29
					2872.4	0.118
					2938.9	0.057

$^{56}\text{Co}$ (0.0)	77.236 d	$\epsilon : 100\%$	$^{56}\text{Fe}(\text{d},2\text{n})$ $^{57}\text{Fe}(\text{d},3\text{n})$ $^{58}\text{Fe}(\text{d},4\text{n})$	-7573 -15219.7 -25264.3	263.434 486.55 733.514 787.743 846.770 852.732 896.510 977.372 996.948 1037.843 1140.368 1159.944 1175.101 1198.888 1238.288 1335.40 1360.212 1771.357 1963.741 2015.215 2034.791 2212.944 2276.131 2598.500	0.0220 0.0540 0.191 0.311 99.9399 0.049 0.073 1.421 0.111 14.05 0.132 0.094 2.252 0.049 66.46 0.1224 4.283 15.41 0.707 3.016 7.77 0.388 0.118 16.97
$^{57}\text{Co}$ (0.0)	271.74 d	$\epsilon : 100\%$	$^{56}\text{Fe}(\text{d},\text{n})$ $^{57}\text{Fe}(\text{d},2\text{n})$ $^{58}\text{Fe}(\text{d},3\text{n})$	3802.9 -3843.2 -13887.8	122.06065 136.47356	85.60 10.68
$^{58}\text{Co}$ (0.0)	70.86	$\epsilon : 100\%$	$^{57}\text{Fe}(\text{d},\text{n})$ $^{58}\text{Fe}(\text{d},2\text{n})$	4729.7 -5314.9	810.7593	99.450

APPENDIX A. TABLES

Table A.3: Products observed in Iridium foils. Iridium has two stable isotopes:  $^{191}\text{Ir}$  (37.3%) and  $^{93}\text{Ir}$  (62.7 %). If the nucleus has provided energy level, the nucleus is an isomer, if nothing then ground state. **The table is inspired by Tarkanyi et al 2019 (ir paper)**

Nuclide level (keV)	Half life	Decay mode	Reaction route	Q value (keV)	$E_\gamma$ (keV)	$I_\gamma$ (%)
$^{188}\text{Ir}$ (0.0)	41.5 h	$\epsilon$ : 100%	$^{191}\text{Ir}(\text{d},4\text{np})$	-24802.0	1209.80	6.9
					1715.67	6.2
					2059.65	7.0
$^{189}\text{Ir}$ (0.0)	13.2 d	$\epsilon$ : 100%	$^{191}\text{Ir}(\text{d},4\text{np})$	-16626.0	95.23	0.38
					216.7	0.52
			$^{193}\text{Ir}(\text{d},5\text{np})$	-30596.0	233.5	0.30
					245.1	6.0
$^{190}\text{Ir}$ (0.0)	11.78 d	$\epsilon$ : 100%	$^{191}\text{Ir}(\text{d},2\text{np})$	-10251.1	294.75	6.6
			$^{193}\text{Ir}(\text{d},4\text{np})$		380.03	2.03
					1036.05	2.42
$^{190m^2}\text{Ir}$ (376.4)	3.087 h	IT:8.6% $\epsilon$ : 91.4%	..	..	361.2	86.72
					502.5	89.38
					616.5	90.14
$^{192}\text{Ir}$ (0.0)	73.829 d	$\epsilon$ : 4.76% $\beta^-$ : 95.24%	$^{191}\text{Ir}(\text{d},\text{p})$	3973.55	201.3112	0.471
					295.95650	28.71
			$^{193}\text{Ir}(\text{d},2\text{np})$	-9996.6	374.4852	0.727
					416.4688	0.670
					468.06885	47.84
					489.06	0.438
					612.46215	5.34
					1061.49	0.0531
$^{194}\text{Ir}$ (0.0)	19.28 h	$\beta^-$ : 100%	$^{194}\text{Ir}(\text{d},\text{p})$	3842.22	293.541	2.5
					300.741	0.35
					589.179	0.140
					938.69	0.60
					1150.75	0.60
					1468.91	0.19
$^{194m^2}\text{Ir}$ (190+X)	171 d	$\beta^-$ : 100%	..	..	338.8	55
					482.6	97
					562.4	35
					687.8	3.6
$^{188}\text{Pt}$ (0.0)	10.16 d	$\epsilon$ : 99.999974% $\alpha$ : $2.6E - 5\%$	$^{191}\text{Pt}(\text{d},2\text{n})$	-26109.0	195.05	18.4
					381.43	7.4
$^{189}\text{Pt}$ (0.0)	10.87 h	$\epsilon$ : 100%	$^{191}\text{Ir}(\text{d},4\text{n})$	-19389.0	94.34	6.5
					113.82	2.5
					243.50	5.9
					317.65	2.8
					721.38	7.9
$^{191}\text{Pt}$ (0.0)	2.802 d	$\epsilon$ : 100%	$^{191}\text{Ir}(\text{d},2\text{n})$	-4017.0	178.96	12.5
					351.17	42.6
			$^{193}\text{Ir}(\text{d},4\text{n})$	-17988.0	409.44	100
					456.47	42
					538.87	181
					624.06	18.5
$^{193m}\text{Pt}$ (149.783)	4.33 d	IT:100%	$^{193}\text{Ir}(\text{d},2\text{n})$	-3063.5	66.831	7.21
					135.5	0.1145475

Table A.4: Products observed on Copper foils. Copper has two stable isotopes:  $^{63}\text{Cu}$  (69.15%) and  $^{65}\text{Cu}$  (30.85 %). If the nucleus has provided energy level, the nucleus is an isomer, if nothing then ground state. **The table is inspired by Tarkanyi et al 2019 (ir paper))**

Nuclide level (keV)	Half life	Decay mode	Reaction route	Q value (keV)	$E_{\gamma}$ (keV)	$I_{\gamma}$ (%)
$^{59}\text{Fe}$ (0.0)	44.490 d	$\beta^-$ : 100%	$^{63}\text{Cu}(\text{d},2\text{p}\alpha)$	-8782.1	1099.245	56.5
			$^{65}\text{Cu}(\text{d},2\alpha)$	1687.0	1291.590	43.2
$^{60}\text{Co}$ (0.0)	1925.28 d	$\beta^-$ : 100%	$^{63}\text{Cu}(\text{d},\text{p}\alpha)$	-507.6	1173.228	99.85
			$^{65}\text{Cu}(\text{d},\text{t}\alpha)$	-9852.4	1332.492	99.9826
$^{61}\text{Co}$ (0.0)	1.649 h	$\beta^-$ : 100%	$^{63}\text{Cu}(\text{d},\text{n}3\text{p})$	-19484.2	67.412	84.7
			$^{65}\text{Cu}(\text{d},\text{np}\alpha)$	-9015.1		
$^{65}\text{Ni}$ (0.0)	2.51719 h	$\beta^-$ : 100%	$^{65}\text{Cu}(\text{d},2\text{p})$	-3580.2	1481.84	23.59
$^{61}\text{Cu}$ (0.0)	3.339 h	$\epsilon$ : 100%	$^{63}\text{Cu}(\text{d},3\text{np})$	-21962.9	282.956	12.2
			$^{65}\text{Cu}(\text{d},5\text{np})$	-39789.4	656.008	10.8
					1185.234	3.7
$^{64}\text{Cu}$ (0.0)	12.701 h	$\epsilon$ : 61.5% $\beta^-$ : 38.5	$^{63}\text{Cu}(\text{d},\text{p})$	5691.54	1345.77	0.475
			$^{65}\text{Cu}(\text{d},2\text{np})$	-12135.0		
$^{62}\text{Zn}$ (0.0)	9.193 h	$\epsilon$ : 100%	$^{63}\text{Zn}(\text{d},3\text{n})$	-15490.0	40.85	25.5
			$^{65}\text{Cu}(\text{d},5\text{n})$	-33316.6	243.36	2.52
					246.95	1.90
					260.43	1.35
					304.88	0.29
					394.03	2.24
					548.35	15.3
					596.56	26.0
					637.41	0.25
$^{63}\text{Zn}$ (0.0)	38.47 m	$\epsilon$ : 100%	$^{63}\text{Cu}(\text{d},2\text{n})$	-6373.3	449.93	0.236
			$^{65}\text{Cu}(\text{d},4\text{n})$	-24199.8	669.62	8.2
					962.06	6.5
$^{65}\text{Zn}$ (0.0)	243.93 d	$\epsilon$ : 100%	$^{65}\text{Cu}(\text{d},2\text{n})$	-4358.6	1115.539	50.04